Available online at www.sciencedirect.com
ScienceDirect
International Journal of Solids and Structures 45 (2008) 1302–1331
INTERNATIONAL JOURNAL OF SOLIDS AND STRUCTURES
www.elsevier.com/locate/ijsolstr

A kinematic FE limit analysis model for thick English bond masonry walls

A. Cecchi [a], G. Milani [b,*]

[a] *IUAV University of Venice Dorsoduro 2206, ex convento Terese, 30123 Venezia, Italy*
[b] *Department of Engineering, University of Ferrara, Via Saragat 1, 44100 Ferrara, Italy*

Received 30 April 2007; received in revised form 27 August 2007
Available online 1 October 2007

Abstract

Two-wythes masonry walls arranged in English bond texture were often used in the past as bearing panels in seismic area. On the other hand, earthquake surveys have demonstrated that masonry strength under horizontal actions is usually insufficient, causing premature collapses of masonry buildings, often ascribed to out-of-plane actions. Furthermore, many codes of practice impose for new brickwork walls a minimal slenderness, which for instance is fixed by the Italian O.P.C.M. 3431 equal to 12 for artificial bricks and 10 for natural blocks masonry.

For the above reasons, the analysis at failure of English bond brickwork walls under out-of-plane actions is a topic that deserves consideration, despite the fact that almost the totality of the studies of masonry at failure is devoted to running bond arrangements. Furthermore, it must be noted that an approach based on the analysis of running bond texture – in comparison with English bond pattern – is not suitable for the investigation of the behavior of bearing panels.

In this framework, in the present paper, a Reissner–Mindlin kinematic limit analysis approach is presented for the derivation of the macroscopic failure surfaces of two-wythes masonry arranged in English bond texture. In particular, the behavior of a 3D system constituted by infinitely resistant bricks connected by joints reduced to interfaces with frictional behavior and limited tensile/compressive strength is identified with a 2D Reissner–Mindlin plate. In this way, assuming both an associated flow rule for the constituent materials and a finite subclass of possible deformation modes, an upper bound approximation of macroscopic English bond masonry failure surfaces is obtained as a function of macroscopic bending moments, torsion and shear forces.

Several examples of technical relevance are treated both at a cell level and at a structural level, addressing the differences in terms of collapse loads and failure surfaces due to different textures and constituent laws for joints. Finally, two meaningful structural examples consisting of a panel in cylindrical flexion and a masonry slab constrained at three edges and out-of-plane loaded are discussed. A detailed comparison in terms of deformed shapes at collapse and failure loads between a 2D FE Reissner–Mindlin limit analysis approach and a full 3D heterogeneous FE model shows the reliability of the results obtained using the kinematic identification approach proposed.

Keywords: Masonry; Reissner–Mindlin plates; English bond; Limit analysis; Out-of-plane loads

* Corresponding author. Tel.: +39 0532 974911; fax: +39 0532 974870.
E-mail address: gmilani@ing.unife.it (G. Milani).

0020-7683/$ - see front matter © 2007 Elsevier Ltd. All rights reserved.
doi:10.1016/j.ijsolstr.2007.09.019

1. Introduction

Consolidated rules of thumbs used for centuries by European technicians suggest to prevent premature loss of equilibrium of masonry elements subjected to horizontal loads by reducing their slenderness. Following this principle, many codes of practice impose for new brickwork walls a minimal height/thickness ratio, which is for instance fixed by the Italian O.P.C.M. 3431 (2005) equal to 12 for artificial bricks and 10 for natural blocks masonry.

As a consequence, existing and new masonry structures in European seismic areas can be build in multi-wythes thickness arrangements, being English and Flemish bond two of the most diffused patterns.

On the other hand, the inadequate resistance of brickwork under out-of-plane loads is well known. Such actions are usually related to seismic events and represent a primary cause of failure in different typologies of masonry, especially for historical buildings (see for instance Spence and Coburn, 1992). Related to this problem, another relevant aspect that should be considered is the important role held by vertical compressive membrane actions on out-of-plane strength. As a rule, in fact, vertical loads (either self weight and permanent loads) are not negligible and increase both the ultimate out-of-plane strength and the ductility of masonry, bringing additional complexity to the structural analyses.

Despite the considerable efforts made in the last decade for the analysis at collapse of masonry elements out-of-plane loaded, almost the totality of these studies is devoted to running bond textures. On the contrary, there is still a lack of knowledge concerning multi-wythes thickness walls, probably due to complexity of possible numerical models, closely related to the high number of variables involved when standard heterogeneous FE non-linear analyses are performed. Moreover, other two important aspects of masonry at failure that preclude the utilization of standard FE codes is the anisotropy (Milani et al., 2006a), closely related to the constituent materials (mortar and bricks) and the bond pattern, and the limited compressive strength, which is independent from shear strength, as demonstrated experimentally by Page (1981).

For the above reasons, the analysis at failure of English bond brickwork walls subjected to out-of-plane actions is a topic that deserves consideration. In particular, a model based on a simplified kinematically admissible homogenization approach and limit analysis seems particularly attractive, since the actual arrangement of bricks and mortar can be considered only at a cell level.

Furthermore, a limit analysis approach requires only a reduced number of material parameters and is able to provide as output information limit multipliers of loads, failure mechanisms and, at least on critical sections, the stress distribution at collapse (see Sutcliffe et al., 2001).

In this framework, in the present paper, a kinematic limit analysis approach in which $(-a)$ bricks are supposed infinitely resistant and $(-b)$ joints are reduced to interfaces, is used in order to have a realistic prediction of the actual behavior at failure of panels out-of-plane loaded. It is worth noting that models based on the homogenization theory have been presented under the same hypotheses by de Buhan and de Felice (1997) for in-plane loaded walls and by Cecchi et al. (2007) for out-of-plane loaded running bond plates. In both cases, an associated flow rule for joints was adopted, despite the fact that frictional phenomena may require the adoption of non-associated plasticity for the constituent materials (Ferris and Tin-Loi, 2001; Orduña and Lourenço, 2005).

Nevertheless, at present, we have not at disposal theorems regarding homogenization of rigid plastic materials with non-associated flow rule, even if calculations could be carried out, given a friction and a dilation angles for mortar, with an "effective" friction and associated flow rules (Drescher and Detournay, 1993).

On the other hand, the adoption of non-associated plasticity implies the lack of the uniqueness of the solution, i.e. that a multiplicity of solutions can exist for these limit analysis problems (see Begg and Fishwick, 1995). On the contrary, when associated plasticity is adopted for the constituent materials, homogenization theory can be used in combination with limit analysis (as suggested by Suquet, 1983) for the evaluation of the macroscopic strength domains and simple linear programming problems (easily manageable by means of standard packages) are obtained.

Following the general procedure adopted by the authors for running bond textures (Cecchi et al., 2007), in this paper a simple micro-mechanical model for the kinematic limit analysis of English bond walls out-of-plane loaded under Reissner–Mindlin plate hypotheses is presented.

In analogy to what proposed for running bond textures, a 3D system of infinitely resistant bricks interacting through mortar joints reduced to interfaces is identified with a rigid-plastic homogeneous and anisotropic

Reissner–Mindlin plate. For joints, a Mohr–Coulomb failure criterion with tension cut-off and compressive limited strength is adopted. For English bond pattern, a full description of the model can be given considering a representative volume constituted by four bricks disposed in three rows interacting with the neighbor bricks. In order to obtain a Reissner–Mindlin equivalent plate, a sub-class of motions for the representative volume is a-priori assumed, including horizontal and vertical flexion, torsion and out-of-plane sliding.

Then, a numerical procedure of identification between the 3D discrete Lagrangian system and a continuum equivalent model is imposed in terms of power dissipated in the 3D discrete model and in the continuum.

Since internal dissipation can take place only at the interface between bricks, a simple linear programming problem in few variables is obtained. In this way, macroscopic masonry failure surfaces are numerically evaluated as a function of the macroscopic bending and torsional moments and out-of-plane shear forces. It is worth mentioning that the number of possible failure modes of the English bond elementary cell subjected to a fixed macroscopic action is higher if compared with the running bond case. In particular, internal plastic dissipation can occur for a variety of relative movements between different adjoining bricks.

In Section 2, the basic assumptions adopted for the identification model are presented with particular emphasis on the multi-wythes case, whereas in Section 3 the constrained minimization problem used for obtaining macroscopic failure surfaces is reported.

In Section 4, the micro-mechanical model is applied for some cases of technical interest for the evaluation of the out-of-plane macroscopic failure surfaces of masonry arranged in English bond texture. The important role of vertical membrane compressive load is addressed assuming two different constitutive laws for joint reduced to interfaces. Furthermore, a comparison with running bond failure surfaces is reported. Finally, in Section 5 two meaningful structural examples consisting of a panel in cylindrical flexion and a masonry slab simply supported at two edges, clamped at the base and out-of-plane loaded are discussed. A detailed comparison in terms of deformed shapes at collapse and failure loads between a 2D FE Reissner–Mindlin limit analysis approach and a full 3D heterogeneous FE model shows the reliability of the results obtained using the compatible identification approach proposed.

2. Compatible model for English bond texture

Let an English bond masonry wall be considered with infinitely resistant blocks connected by mortar joints reduced to interfaces with rigid-plastic behavior (Fig. 1). For the case here analyzed, a symmetry middle plane along the thickness of the wall can be identified without difficulties. Thus, a plate and shell model with uncoupled membrane and flexural actions and referred to masonry middle plane can be developed. According to a previous work by the authors (Cecchi et al., 2007), in the discrete system the kinematic is described with reference to a generic couple of blocks. The compatible equivalent model is based on a correspondence between equivalent class of motions in a 3D discrete blocks system and a plate continuous model.

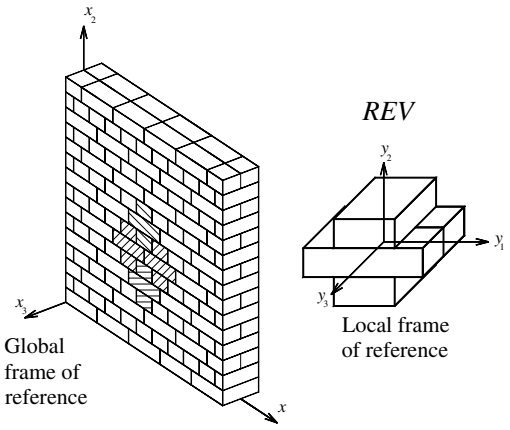

Fig. 1. English bond masonry wall with joints reduced to interfaces and representative volume element chosen for the compatible identification proposed.

A portion of a $\mathcal{P}$ masonry panel (continuous model) with the same dimensions of the REV (discrete block system model) is considered. This portion is chosen so that its center $\mathbf{g}^c$ coincides with the center of the REV. A portion of plate $\mathcal{H}$, with the same edge is considered, so that the $\mathbf{x}$ point of $\mathcal{H}$ coincides with $\mathbf{g}^c$ (Figs. 2–4).

In the discrete system, the motion of a generic couple of blocks $\mathcal{A}$ and $\mathcal{B}$ may be described as a function of their center velocity $\mathbf{w}^a$, $\mathbf{w}^b$ and their angular velocity $\mathbf{\Omega}^a$, $\mathbf{\Omega}^b$. Let $\mathbf{p}$ be the center of the I interface between $\mathcal{A}$ and $\mathcal{B}$. The velocity of the material points $\mathbf{x}$ of $\mathcal{A}$ and $\mathcal{B}$ in contact in a position $\boldsymbol{\xi} \in I$, may be written as:

$$\begin{aligned} \mathbf{w}^a(\mathbf{x}) &= \mathbf{w}^a(\mathbf{p}) + \mathbf{\Omega}^a(\boldsymbol{\xi} - \mathbf{p}) \\ \mathbf{w}^b(\mathbf{x}) &= \mathbf{w}^b(\mathbf{p}) + \mathbf{\Omega}^b(\boldsymbol{\xi} - \mathbf{p}) \end{aligned} \tag{1}$$

Jump of the velocity field $\mathbf{w}(\boldsymbol{\xi})$ between A and B in a point $\boldsymbol{\xi} \in I$ that represents the measure of strain velocity may be written as:

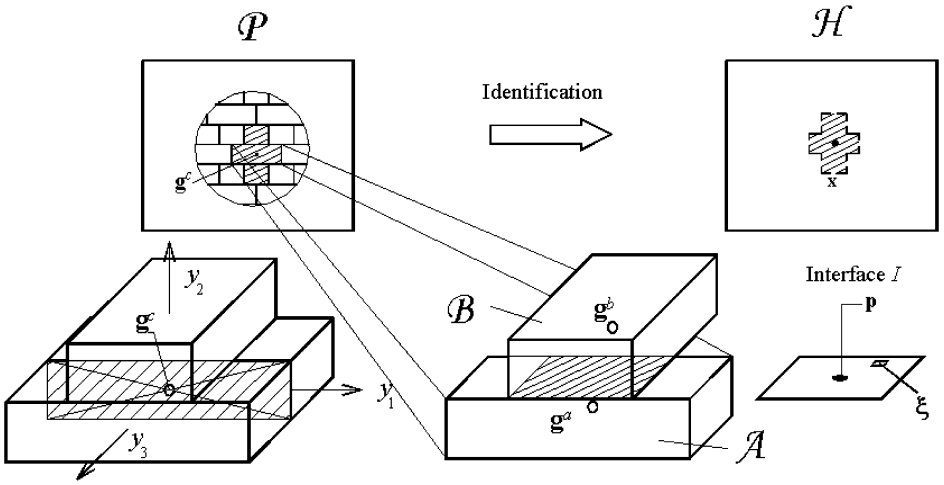

Fig. 2. Procedure of identification between 3D discrete model and 2D plate.

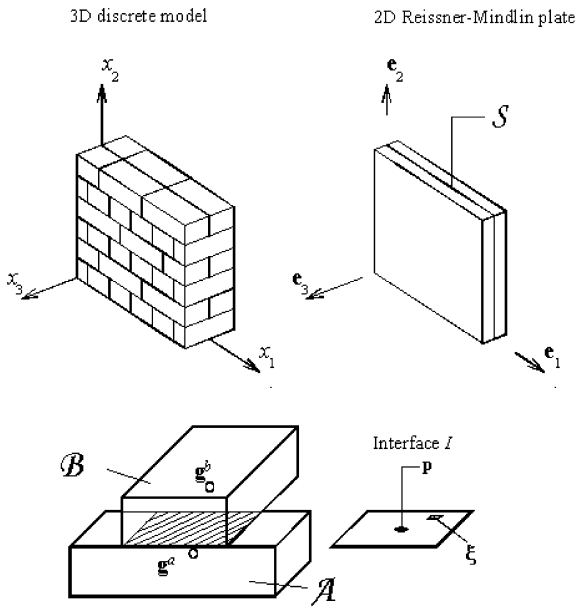

Fig. 3. Geometrical description of the model; two adjacent bricks ($\mathbf{g}^a$ and $\mathbf{g}^b$) connected with a mortar interface I where plastic dissipation occurs.

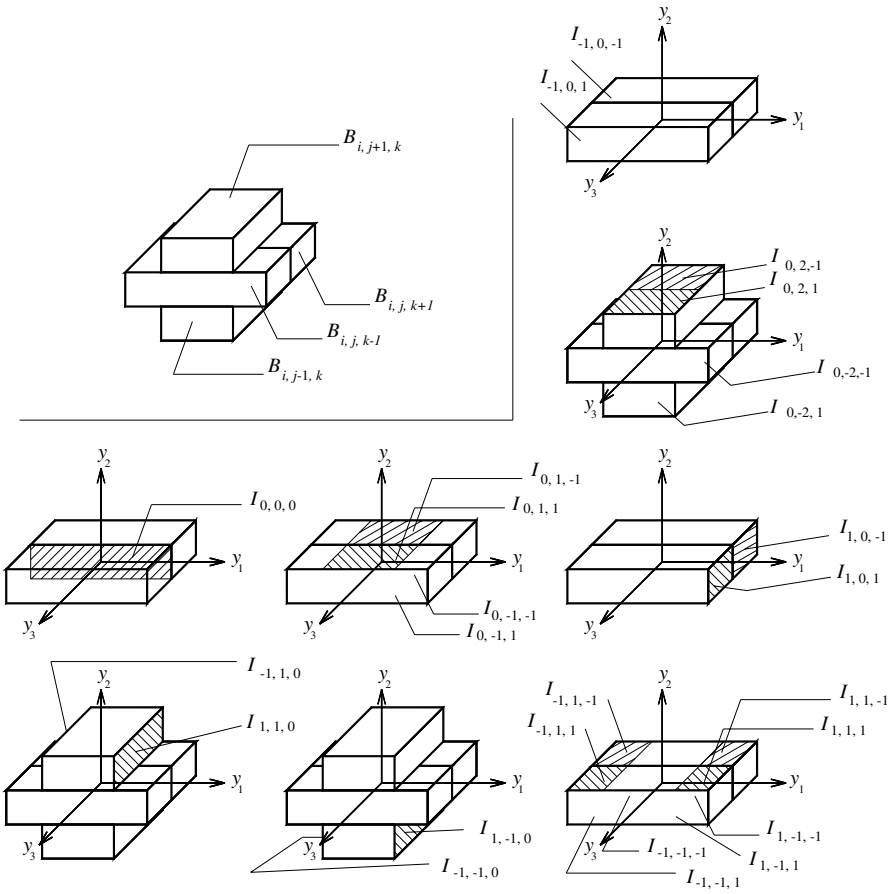

Fig. 4. Mortar interfaces definition.

$$\lfloor \mathbf{w}(\boldsymbol{\xi}) \rfloor = \mathbf{w}^b(\boldsymbol{\xi}) - \mathbf{w}^a(\boldsymbol{\xi}) = \mathbf{w}^b(\mathbf{p}) - \mathbf{w}^a(\mathbf{p}) + \boldsymbol{\Omega}^b(\boldsymbol{\xi} - \mathbf{p}) - \boldsymbol{\Omega}^a(\boldsymbol{\xi} - \mathbf{p}) = \mathbf{w}_p + \boldsymbol{\Omega}_p(\boldsymbol{\xi} - \mathbf{p}) \tag{2}$$

where $\mathbf{w}_p = \mathbf{w}^b(\mathbf{p}) - \mathbf{w}^a(\mathbf{p})$ and $\boldsymbol{\Omega}_p = \boldsymbol{\Omega}^b - \boldsymbol{\Omega}^a$.

Side by side for the panel, a 2D plate model is introduced independently from the discrete 3D model. The plate is identified by its middle plane $\mathcal{S}$ of normal $\mathbf{e}_3$ (Fig. 3).

In a parallel manner, respect to the discrete model, in a plate continuum model the generic motion is described by the following fields:

$$\begin{aligned} &\mathbf{w}(\mathbf{x}) \\ &\boldsymbol{\Omega}(\mathbf{x}) \end{aligned} \tag{3}$$

where $\mathbf{w}(\mathbf{x})$ and $\boldsymbol{\Omega}(\mathbf{x})$ are the velocity vector and angular velocity tensor of the material point $\mathbf{x}$, respectively.

Hence it is possible to assign a correspondence between a class of regular motions in $\mathcal{P}$ and $\mathcal{H}$. The velocity and angular velocity of the center of the brick $\mathcal{A}$ and $\mathcal{B}$ in the discrete system and velocity and angular velocity of the center of the REV in the continuum model are equal:

$$\begin{aligned} \mathbf{w}^a(\mathbf{x}) &= \mathbf{w}(\mathbf{x}) + \operatorname{grad}\mathbf{w}(\mathbf{x})(\mathbf{g}^a - \mathbf{x}) \\ \boldsymbol{\Omega}^a(\mathbf{x}) &= \boldsymbol{\Omega}(\mathbf{x}) + \operatorname{grad}\boldsymbol{\Omega}(\mathbf{x})(\mathbf{g}^a - \mathbf{x}) \end{aligned} \tag{4}$$

and

$$\begin{aligned} \mathbf{w}^b(\mathbf{x}) &= \mathbf{w}(\mathbf{x}) + \operatorname{grad}\mathbf{w}(\mathbf{x})(\mathbf{g}^b - \mathbf{x}) \\ \boldsymbol{\Omega}^b(\mathbf{x}) &= \boldsymbol{\Omega}(\mathbf{x}) + \operatorname{grad}\boldsymbol{\Omega}(\mathbf{x})(\mathbf{g}^b - \mathbf{x}) \end{aligned} \tag{5}$$

where $\mathbf{g}^a$ and $\mathbf{g}^b$ are the center of the $\mathcal{A}, \mathcal{B} \in \mathcal{P}$ generic couple of bricks and a first order Taylor approximation (first order identification) in the velocity and angular velocity is used In the discrete system, the contact forces between blocks $\mathcal{A}$ and $\mathcal{B}$ are $\mathbf{t}^a(\xi)$ and $\mathbf{t}^b(\xi)$ for $\xi \in I$. Equilibrium condition requires that $\mathbf{t}^a(\xi) = -\mathbf{t}^b(\xi)$. Hence, −set $\mathbf{t}^b(\xi) = \mathbf{t}\ (\xi)$, the power dissipated at the interface is:

$$\pi = \int_I \mathbf{t}^a(\xi) \cdot \mathbf{w}^a(\xi) + \mathbf{t}^b(\xi) \cdot \mathbf{w}^b(\xi) = \int_I \mathbf{t}(\xi) \cdot [\mathbf{w}^b(\xi) - \mathbf{w}^a(\xi)] = \mathbf{t}_p \cdot \mathbf{w}_p + \mathbf{\Omega}_p \cdot \int_I \operatorname{skw} \mathbf{t} \otimes (\xi - \mathbf{p}) \tag{6}$$

Set $\mathbf{t}_p = \int_I \mathbf{t}(\xi)$ and $\mathbf{M}_p = 2\int_I \operatorname{skw} \mathbf{t} \otimes (\xi - \mathbf{p})$, Eq. (6) can be written as follows:

$$\pi_p = \mathbf{t}_p \cdot \mathbf{w}_p + \frac{1}{2}\mathbf{M}_p \cdot \mathbf{\Omega}_p \tag{7}$$

Let us define the vector $\mathbf{t}_p$ as $\mathbf{t}_p = \bar{\mathbf{t}}_p + \mathbf{t}_{3p} = [\, t_{1p} \quad t_{2p} \quad 0\,]^{\mathrm{T}} + [\, 0 \quad 0 \quad t_{3p}\,]^{\mathrm{T}}$ where $\bar{\mathbf{t}}_p$ denotes the projection on $\mathcal{S}$ of $\mathbf{t}_p$ and $\mathbf{t}_{3p}$ is the component orthogonal to $\mathcal{S}$ of $\mathbf{t}_p$. Taking into consideration correspondent motion tests, from Eqs. (4) and (5), Eq. (7) may be written as:

$$\begin{aligned} \mathbf{t}_p \cdot \mathbf{w}_p &= \bar{\mathbf{t}}_p \otimes (\mathbf{g}^b - \mathbf{g}^a) \cdot (\operatorname{grad} \bar{\mathbf{w}}) + \mathbf{t}_{3p}(\mathbf{g}^b - \mathbf{g}^a) \cdot (\operatorname{grad} w_3 + \mathbf{\Omega}\mathbf{e}_3) \\ &\quad + \mathbf{t}_{3p}[(\mathbf{p} - \mathbf{g}^a) \otimes (\mathbf{g}^a - \mathbf{x}) - (\mathbf{p} - \mathbf{g}^b) \otimes (\mathbf{g}^b - \mathbf{x})] \cdot (\operatorname{grad} \mathbf{\Omega}\mathbf{e}_3) \end{aligned} \tag{8}$$

$$\begin{aligned} \frac{1}{2}\mathbf{M}_p \cdot \mathbf{\Omega}_p &= \int_I (\mathbf{t}(\xi) \otimes \mathbf{d}_p - \mathbf{d}_p \otimes \mathbf{t}(\xi)) \cdot (\operatorname{grad} \mathbf{\Omega})(\mathbf{g}^b - \mathbf{g}^a) \\ &= \frac{1}{2}\int_I (d_{3p}\bar{\mathbf{t}}(\xi) - t_3(\xi)\bar{\mathbf{d}}_p) \otimes (\mathbf{g}^b - \mathbf{g}^a)(\operatorname{grad} \mathbf{\Omega}\mathbf{e}_3) \end{aligned} \tag{9}$$

where the distance vector $\mathbf{d}_p$ can be written as $\mathbf{d}_p = \xi - \mathbf{p}$. According to the previous notation $\mathbf{d}_p$ may be decomposed as $\mathbf{d}_p = \bar{\mathbf{d}}_p - \mathbf{d}_{3p}$

In the same manner, for the continuum, set $\mathbf{N}$ membrane and shear actions and $\mathbf{M}$ bending and torsion.The mechanical power evaluated on $\mathcal{S}$ may be written as:

$$\pi = \mathbf{N} \cdot \operatorname{sym}(\operatorname{grad} \mathbf{w}) + (\mathbf{N}\mathbf{e}_3 \otimes \mathbf{e}_3) \cdot \mathbf{W} + \mathbf{M} \cdot \operatorname{sym}(\operatorname{grad} \mathbf{\Omega}\mathbf{e}_3) \tag{10}$$

where grad represents the gradient operator on $\mathcal{S}$. Total internal power dissipated can be evaluated as the sum of power dissipated by membrane actions, plate shear actions, bending and torsional moments. In particular, by indicating with an upper line the projection on $\mathcal{S}$, the previous equation becomes:

$$\pi = \overline{\mathbf{N}} \cdot \operatorname{sym}(\operatorname{grad} \bar{\mathbf{w}}) + \mathbf{T} \cdot (\operatorname{grad} w_3 + \mathbf{\Omega}\mathbf{e}_3) + \mathbf{M} \cdot \operatorname{sym}(\operatorname{grad} \mathbf{\Omega}\mathbf{e}_3) \tag{11}$$

In what follows we assume:

- $\operatorname{sym}(\operatorname{grad} \bar{\mathbf{w}}) = \dot{\mathbf{E}}$, where $\dot{\mathbf{E}}$ is the in-plane membrane strain rate tensor;
- $\operatorname{sym}(\operatorname{grad} \mathbf{\Omega}\mathbf{e}_3) = \dot{\boldsymbol{\chi}}$, where $\dot{\boldsymbol{\chi}}$ is the curvature rate tensor ($\dot{\chi}_{\alpha\beta} = 1/2(\omega_{\alpha,\beta} + \omega_{\beta,\alpha})$ with $\alpha, \beta = 1, 2$);
- $\operatorname{grad} w_3 + \mathbf{\Omega}\mathbf{e}_3 = \dot{\boldsymbol{\gamma}} = [\, \dot{\gamma}_{13} \quad \dot{\gamma}_{23}\,]^{\mathrm{T}}$, where $\dot{\boldsymbol{\gamma}}$ is the shear strain rate vector.

Furthermore, $\overline{N}$ represents the membrane actions tensor, $\mathbf{N}\mathbf{e}_3 = \mathbf{T}$ represents the shear actions vector and $\mathbf{M}$ represents the bending moments and torsion tensor. It must be noted that the angular velocity tensor $\mathbf{\Omega}(\mathbf{x})$ in the case of a plate model is: ω_α with the Greek index $\alpha = 1, 2$. In fact, as well known ω_3 component is equal to zero in the case of plate model.

At this stage, for a chosen REV and a given class of regular motions, we impose that the mechanical power dissipated by the contact actions on $\mathcal{P}$ and $\mathcal{H}$ coincides. Under these assumptions, the membrane and moment tensors $\overline{\mathbf{N}}$ and $\mathbf{M}$, as well as plate shear vector $\mathbf{T}(\mathbf{T} = \mathbf{N}\mathbf{e}_3)$ may be expressed as a function of the vector $\mathbf{t}_p$, i.e. of the measure of the stress in the micro-mechanical model.

$$\begin{aligned}
\overline{\mathbf{N}} &= \frac{1}{2A}\sum_n \operatorname{sym}\bar{\mathbf{t}}_p \otimes (\mathbf{g}^b - \mathbf{g}^a) \\
\mathbf{T} &= \frac{1}{2A}\sum_n \mathbf{t}_{3p}(\mathbf{g}^b - \mathbf{g}^a) \\
\mathbf{M} &= \frac{1}{2A}\left[\sum_n \mathbf{t}_{3p}\operatorname{sym}[(\mathbf{p}-\mathbf{g}^a)\otimes(\mathbf{g}^a-\mathbf{x}) - (\mathbf{p}-\mathbf{g}^b)\otimes(\mathbf{g}^b-\mathbf{x})]\right] \\
&\quad + \sum_n \int_I \operatorname{sym}[d_{3p}\bar{\mathbf{t}}(\boldsymbol{\xi}) - t_3(\boldsymbol{\xi})\bar{\mathbf{d}}_p]\otimes(\mathbf{g}^b-\mathbf{g}^a)]
\end{aligned} \tag{12}$$

where A is the area of the chosen REV and the symbol $\sum$ indicates a summation extended to all the interfaces to which the chosen REV is in contact. It must be noted that the part of π associated to $\operatorname{skw}\{\operatorname{grad}\mathbf{W}\}$ and to $\operatorname{skw}\{\operatorname{grad}\mathbf{We}_3\}$ is not taken into account. In fact, in the adopted plate model these kinematic fields characterize neutral (rigid) motions.

The 1/2 coefficient which appears in the above expressions for **N**, **T** and **M** is relative only to the externals interfaces of the REV – the power dissipated at the interface between two REVs involves both REVs – while in the case of interfaces internal to the REV the coefficient for **N**, **T** and **M** is 1.

2.1. The multi-wythes masonry case

In this section, the derivation of a plate model for English bond masonry is presented as a simple application of the proposed theory. In the follows the procedure adopted by the authors (Cecchi et al., 2007) for the definition of 3D discrete model is used.

It is worth noting that the procedure followed in this paper is not based on rigorous homogenization theory, but it represents a straightforward approach of identification between 3D discrete model and 2D Reissner–Mindlin plate. The application of classic homogenization is avoided in order to put at disposal to practitioners a technically simple kinematically admissible model. The a-priori assumption of a sub-class of regular motions in the RVE, representing a number of most probable elementary failure mechanisms which can occur in practice, simplifies the formulation to a great extent, giving the possibility of symbolically handle the optimization problem at a cell level. From a theoretical point of view, such macroscopic motions have to be homogeneous. In this way, the model obtained is compatible (but not necessarily equilibrated) and the introduction of periodic velocity fields, required by rigorous homogenization theory, can be circumvented.Therefore, even if the simple model proposed is far to be rigorous, it can be profitably used by practitioners for structural analyses at collapse.

From the above considerations, in fact, the following advantages of the procedure proposed can be underlined: (1) its simplicity in terms of formulation; (2) the possibility to implement directly the procedure in a FE limit analysis code for the evaluation of collapse loads of entire walls; (3) its ability to provide in any case upper bound approximations of the actual masonry strength domain.

Differently from the simple running bond case, the chosen REV is constituted by four blocks. In this case, the center of the REV corresponds to origin of the local frame of references, as shown in Fig. 1.

In order to evaluate expressions (12), 5 internal interfaces (1 in the thickness of the plate $I_{0,0,0}$, and 4 horizontal interfaces $I_{0,k2,k3}$, with $k_1 = k_2 = \pm 1$) and 20 external interfaces (8 bed interfaces and 12 head interfaces) must be taken into account for the evaluation of the total internal power dissipated, Fig. 4. It must be remarked that the internal interfaces spend power in the interior of the REV while the external interfaces spend power for the chosen REV but also in the neighbor REVs (see Fig. 2), hence only 1/2 of its value has to be taken into account in the total internal power dissipation.

Let $\mathbf{g}_{i,j,k}$ be the position of the center of the generic REV in the 3D Euclidean space, b, a and t are brick length, brick height and brick thickness, respectively. The position of the centers of the four blocks that constitute the REV are:

$$g_{0,0,-1} = \begin{pmatrix} 0 \\ 0 \\ -\frac{t}{2} \end{pmatrix}; \quad g_{0,0,+1} = \begin{pmatrix} 0 \\ 0 \\ \frac{t}{2} \end{pmatrix}; \quad g_{+1,0,-1} = \begin{pmatrix} 0 \\ a \\ 0 \end{pmatrix}; \quad g_{-1,0,+1} = \begin{pmatrix} 0 \\ -a \\ 0 \end{pmatrix}$$

Due to the regularity of masonry under consideration, a $\mathbf{B}_{i,j,k}$ block interacts with a $\mathbf{B}_{i+k_1,j+k_2,k+k_3}$ block by means of a I_{k_1,k_2,k_3} joint.

In particular, it is worth noting that for INTERNAL INTERFACES:

– if $k_1 = 0$ and k_2, $k_3 = \pm 1$, then $I_{k_1,k_2,k3}$ represents a horizontal interface;
– if $k_1 = k_2 = k_3 = 0$, then $I_{0,0,0}$ represents the internal interface along the wall thickness.

On the other hand, for EXTERNAL INTERFACES:

– if k_1, $k_2 = \pm 1$ and $k_3 = 0$ then $I_{k_1,k_2,k3}$ represents a vertical interface when only one block is present in the panel thickness;
– if k_1, $k_3 = \pm 1$ and $k_2 = 0$then $I_{k_1,k_2,k3}$ represents a vertical interface when two blocks are present in the panel thickness;
– if k_1, k_2, $k_3 = \pm 1$ and, then I_{k_1,k_2} is a horizontal interface when two blocks are present in the panel thickness;
– if $k_1 = 0$, $k_2 = \pm 2$ and $k_3 = \pm 1$ then $I_{k_1,k_2,k3}$ represents a vertical interface when only one block is present in the panel thickness;

For the sake of simplicity, the following interfaces definitions will be used:

(1) INTERNAL INTERFACES:

$$I_{0,0,0} = \begin{cases} -\frac{b}{2} \leqslant y_1 \leqslant \frac{b}{2} \\ -\frac{a}{2} \leqslant y_2 \leqslant \frac{a}{2}; \\ y_3 = 0 \end{cases} \quad I_{0,-1,-1} = \begin{cases} -\frac{t}{2} \leqslant y_1 \leqslant \frac{t}{2} \\ -\frac{a}{2} = y_2 \\ -t \leqslant y_3 \leqslant 0 \end{cases}; \quad I_{0,-1,+1} = \begin{cases} -\frac{t}{2} \leqslant y_1 \leqslant \frac{t}{2} \\ -\frac{a}{2} = y_2 \\ 0 \leqslant y_3 \leqslant t \end{cases}$$
$$I_{0,+1,-1} = \begin{cases} -\frac{t}{2} \leqslant y_1 \leqslant \frac{t}{2} \\ \frac{a}{2} = y_2 \\ -t \leqslant y_3 \leqslant 0 \end{cases}; \quad I_{0,+1,+1} = \begin{cases} -\frac{t}{2} \leqslant y_1 \leqslant \frac{t}{2} \\ \frac{a}{2} = y_2 \\ 0 \leqslant y_3 \leqslant t \end{cases} \tag{13}$$

(2) EXTERNAL INTERFACES:Vertical interfaces when only one brick is present in the panel thickness

$$I_{+1,+1,0} = \begin{cases} y_1 = \frac{t}{2} \\ \frac{a}{2} \leqslant y_2 \leqslant \frac{3a}{2} \\ -t \leqslant y_3 \leqslant t \end{cases}; \quad I_{+1,-1,0} = \begin{cases} y_1 = \frac{t}{2} \\ -\frac{3a}{2} \leqslant y_2 \leqslant -\frac{a}{2}; \\ -t \leqslant y_3 \leqslant t \end{cases} \quad I_{-1,+1,0} = \begin{cases} y_1 = -\frac{t}{2} \\ \frac{a}{2} \leqslant y_2 \leqslant \frac{3a}{2} \\ -t \leqslant y_3 \leqslant t \end{cases};$$
$$I_{-1,-1,0} = \begin{cases} y_1 = -\frac{t}{2} \\ -\frac{3a}{2} \leqslant y_2 \leqslant -\frac{a}{2} \\ -t \leqslant y_3 \leqslant t \end{cases} \tag{14}$$

Vertical interfaces when two bricks are present in the panel thickness

$$I_{-1,0,-1} = \begin{cases} y_1 = -\frac{b}{2} \\ -\frac{a}{2} \leqslant y_2 \leqslant \frac{a}{2}; \\ -t \leqslant y_3 \leqslant 0 \end{cases} \quad I_{-1,0,+1} = \begin{cases} y_1 = -\frac{b}{2} \\ -\frac{a}{2} \leqslant y_2 \leqslant \frac{a}{2}; \\ 0 \leqslant y_3 \leqslant t \end{cases} \quad I_{+1,0,-1} = \begin{cases} y_1 = \frac{b}{2} \\ -\frac{a}{2} \leqslant y_2 \leqslant \frac{a}{2}; \\ -t \leqslant y_3 \leqslant 0 \end{cases}$$
$$I_{+1,0,+1} = \begin{cases} y_1 = -\frac{b}{2} \\ -\frac{a}{2} \leqslant y_2 \leqslant \frac{a}{2} \\ 0 \leqslant y_3 \leqslant t \end{cases} \tag{15}$$

Horizontal interfaces when two bricks are present in the panel thicknesss

$$I_{+1,+1,+1}=\begin{cases}\frac{t}{2}\leqslant y_1\leqslant\frac{b}{2}\\ y_2=\frac{a}{2}\\ 0\leqslant y_3\leqslant t\end{cases};\quad I_{+1,+1,-1}=\begin{cases}\frac{t}{2}\leqslant y_1\leqslant\frac{b}{2}\\ y_2=\frac{a}{2}\\ -t\leqslant y_3\leqslant 0\end{cases};\quad I_{+1,-1,+1}=\begin{cases}\frac{t}{2}\leqslant y_1\leqslant\frac{b}{2}\\ y_2=-\frac{a}{2}\\ 0\leqslant y_3\leqslant t\end{cases};$$
$$I_{+1,-1,-1}=\begin{cases}\frac{t}{2}\leqslant y_1\leqslant\frac{b}{2}\\ y_2=-\frac{a}{2}\\ -t\leqslant y_3\leqslant 0\end{cases};\quad I_{-1,+1,+1}=\begin{cases}-\frac{b}{2}\leqslant y_1\leqslant-\frac{t}{2}\\ y_2=\frac{a}{2}\\ 0\leqslant y_3\leqslant t\end{cases};\quad I_{-1,+1,-1}=\begin{cases}-\frac{b}{2}\leqslant y_1\leqslant-\frac{t}{2}\\ y_2=\frac{a}{2}\\ -t\leqslant y_3\leqslant 0\end{cases};\tag{16}$$
$$I_{-1,-1,+1}=\begin{cases}-\frac{b}{2}\leqslant y_1\leqslant-\frac{t}{2}\\ y_2=-\frac{a}{2}\\ 0\leqslant y_3\leqslant t\end{cases};\quad I_{-1,-1,-1}=\begin{cases}-\frac{b}{2}\leqslant y_1\leqslant-\frac{t}{2}\\ y_2=-\frac{a}{2}\\ -t\leqslant y_3\leqslant 0\end{cases}$$

Horizontal interfaces when two bricks are present in the panel thickness

$$I_{0,+2,+1}=\begin{cases}-\frac{t}{2}\leqslant y_1\leqslant\frac{t}{2}\\ y_2=\frac{3a}{2}\\ 0\leqslant y_3\leqslant t\end{cases};\quad I_{+1,+2,-1}=\begin{cases}-\frac{t}{2}\leqslant y_1\leqslant\frac{t}{2}\\ y_2=\frac{3a}{2}\\ -t\leqslant y_3\leqslant 0\end{cases};\quad I_{0,-2,+1}=\begin{cases}-\frac{t}{2}\leqslant y_1\leqslant\frac{t}{2}\\ y_2=-\frac{3a}{2}\\ 0\leqslant y_3\leqslant t\end{cases};$$
$$I_{+1,-2,-1}=\begin{cases}-\frac{t}{2}\leqslant y_1\leqslant\frac{t}{2}\\ y_2=-\frac{3a}{2}\\ -t\leqslant y_3\leqslant 0\end{cases}\tag{17}$$

As a rule, the jump of velocity between two adjacent blocks may be written as follows:

$$[\mathbf{w}^{k_1,k_2}]=\Delta\mathbf{w}^{k_1,k_2}+\Delta\boldsymbol{\Omega}^{k_1,k_2}(\mathbf{g}^{i+k_1,j+k_2}-\mathbf{g}^{i,j})\tag{18}$$

where Δ represent the difference operator.

According to Cecchi and Sab (2004) and Cecchi and Rizzi (2003), starting from Eqs. (1) (3) and (4) (5), the identification between 3D discrete model and 2D continuum model has been obtained assuming:

$$\begin{aligned}&\mathbf{w}^{i,j}=\mathbf{w}(\mathbf{g}^{i,j})\\ &\Omega_{32}^{i,j}=\omega_1(\mathbf{g}^{i,j})\\ &\Omega_{31}^{i,j}=-\omega_2(\mathbf{g}^{i,j})\\ &\Omega_{12}^{i,j}=0\end{aligned}\tag{19}$$

It is worth noting that in the Reissner–Mindlin model proposed $\Omega_{12}^{i,j}=0$, as shown in Eq. (19).

Fig. 5 shows the effect on the elementary cell of homogeneous in-plane deformations. In this case, the wall behaves similarly to running bond texture. Such behavior is also confirmed by the results of some experimental tests conducted by Calvi et al. (1992) on shear panels arranged in English bond, which differ not drastically with respect to running bond.

Fig. 6a shows the effect on the brickwork of a homogeneous deformation $\omega_{1,1}\neq 0$ with all the other strain measures set to zero. It must be noted that English bond behavior is somewhat different with respect to the running bond one. In this case in fact, both head and bed joints are involved in the dissipation induced by this deformation, as well as the thickness joint. Fig. 6b shows the effect on the brickwork of a homogeneous deformation in which $\omega_{2,2}\neq 0$ and all the other strain measures are set to zero. In this case, it is interesting to note that the wall behaves exactly in the same way with respect to running bond texture, i.e. only the bed joints present a relative jump of velocities between adjacent bricks.

Similarly, in Fig. 6c and d the cases $\omega_{1,2}\neq 0$ and $\omega_{2,1}\neq 0$ are examined. In the first case, no differences occur between English and running bond texture (there is torsion only in the bed joints); in fact, as expected, the behavior is the same along the thickness of the single block case. On the contrary several differences may be noted in the second case, since torsion is present in the head joints, bending moment acts in the bed joints and sliding occurs in the thickness joint.

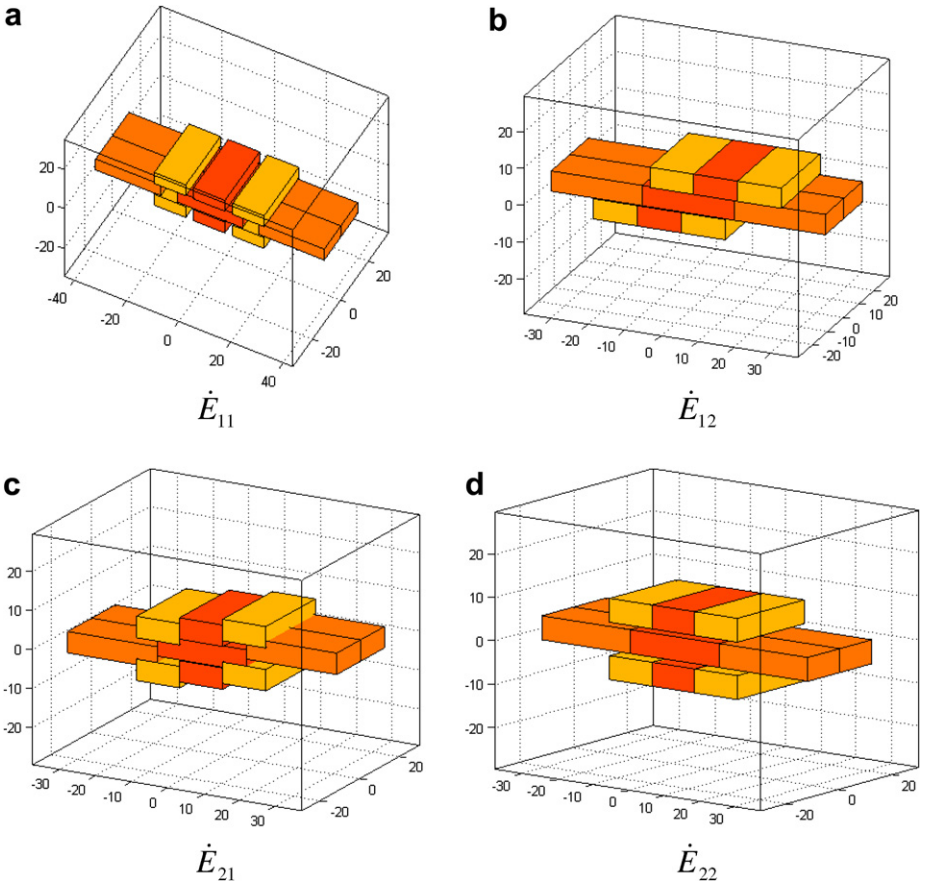

Fig. 5. Elementary in-plane homogeneous deformations applied to the representative volume element. (a) $\dot{E}_{11}$, (b) $\dot{E}_{12}$, (c) $\dot{E}_{21}$, (d) $\dot{E}_{22}$.

Finally, Fig. 7 refers to the evaluation of the shear constants and shows shear deformation rates. In particular, Fig. 7a shows the $\dot{\gamma}_{13}$ component, while Fig. 7b the $\dot{\gamma}_{23}$ component.

3. The linear programming problem at a cell level

In this section, a numerical procedure to obtain macroscopic in- and out-of-plane failure surfaces for multi-wythes masonry is presented. Reissner–Mindlin plate hypotheses with infinitely resistant bricks and joints reduced to interfaces are assumed. For joints, a perfect plastic behavior obeying an associated flow rule is also adopted.

The utilization of classical limit analysis theorems allows the combined utilization of simplified or rigorous homogenization and linear programming. In this framework, Suquet (1983) proved that macroscopic strength domains for periodic arrangements of heterogeneous materials may be obtained assuming a rigid-plastic behavior and associated flow rule for the constituent materials, by means of both static and kinematic theorems of limit analysis. Such approaches have been widely applied for the evaluation of both in-plane (de Buhan and de Felice, 1997; Milani et al., 2006a) and out-of-plane failure surfaces of masonry (Milani et al., 2006b; Sab, 2003; Cecchi et al., 2007) for running bond textures.

On the contrary, at present and despite the great importance of the problem, there is still a lack of knowledge concerning the derivation of the macroscopic failure surfaces for double-wythes thickness masonry panels.

Experimental evidences show that basic failure modes for masonry walls with weak mortar are a mixing of sliding along the joints, direct tensile splitting of the joints and compressive crushing at the interface between

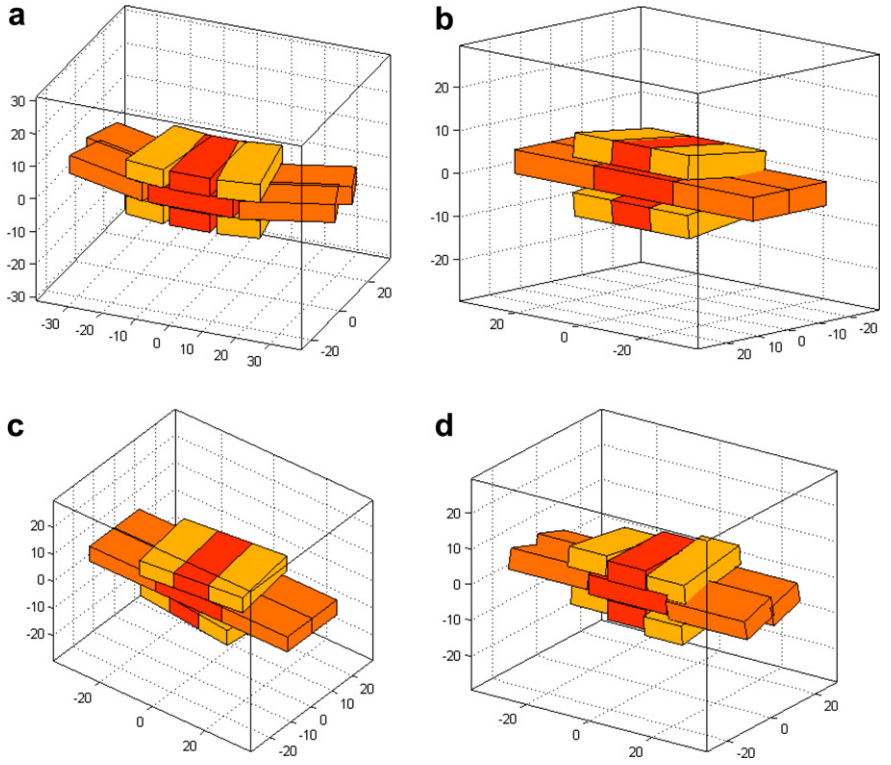

Fig. 6. Elementary homogeneous deformations applied to the representative volume element. (a) $\omega_{1,1} = \dot{\chi}_{11}$. (b) $\omega_{2,2} = \dot{\chi}_{22}$. (c) $\omega_{2,1}$. (d) $\omega_{1,2}$.

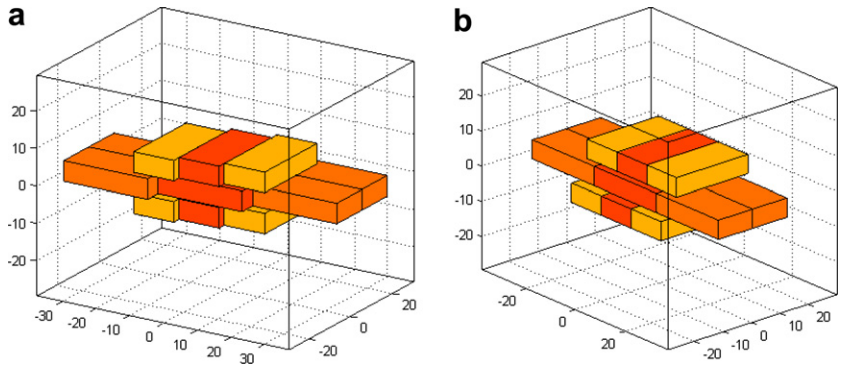

Fig. 7. Shear deformation rates. (a) $\dot{\gamma}_{13} = w_{3,1} + \omega_1$. (b) $\dot{\gamma}_{23} = w_{3,2} + \omega_2$.

mortar and bricks. Thus, a Mohr–Coulomb failure criterion with tension cut-off f_t and a linearized cap in compression (f_c, Φ_2), see Fig. 8 and Lourenço and Rots (1997) is adopted. A classic Mohr–Coulomb failure criterion may be obtained as particular case when $f_t = c/\tan\Phi$ and $f_c \to \infty$.

In the framework of linear programming, a piecewise linear approximation of the failure surface $\phi = \phi(\boldsymbol{\sigma})$ is adopted for each interface I of area A^I, constituted by n_{lin} planes of equation $\mathbf{A}_i^{I^{\mathrm{T}}}\boldsymbol{\sigma} = c_i^I \quad 1 \leqslant i \leqslant n_{lin}$, where $\boldsymbol{\sigma} = [\,\sigma_{33} \quad \sigma_{13} \quad \sigma_{23}\,]$, σ_{33} is the normal stress on the interface and σ_{13} and σ_{23} are tangential stresses along two assigned perpendicular directions, see Fig. 8. In Fig. 8 $\boldsymbol{\xi} = (\xi_1, \xi_2)$ represents the position vector of point $\boldsymbol{\xi}$ in a suitable local frame of reference laying on the interface plane, with axis ξ_3 orthogonal to the interface plane and origin $\mathbf{p}$ corresponding to the centroid of the interface, Fig. 2.

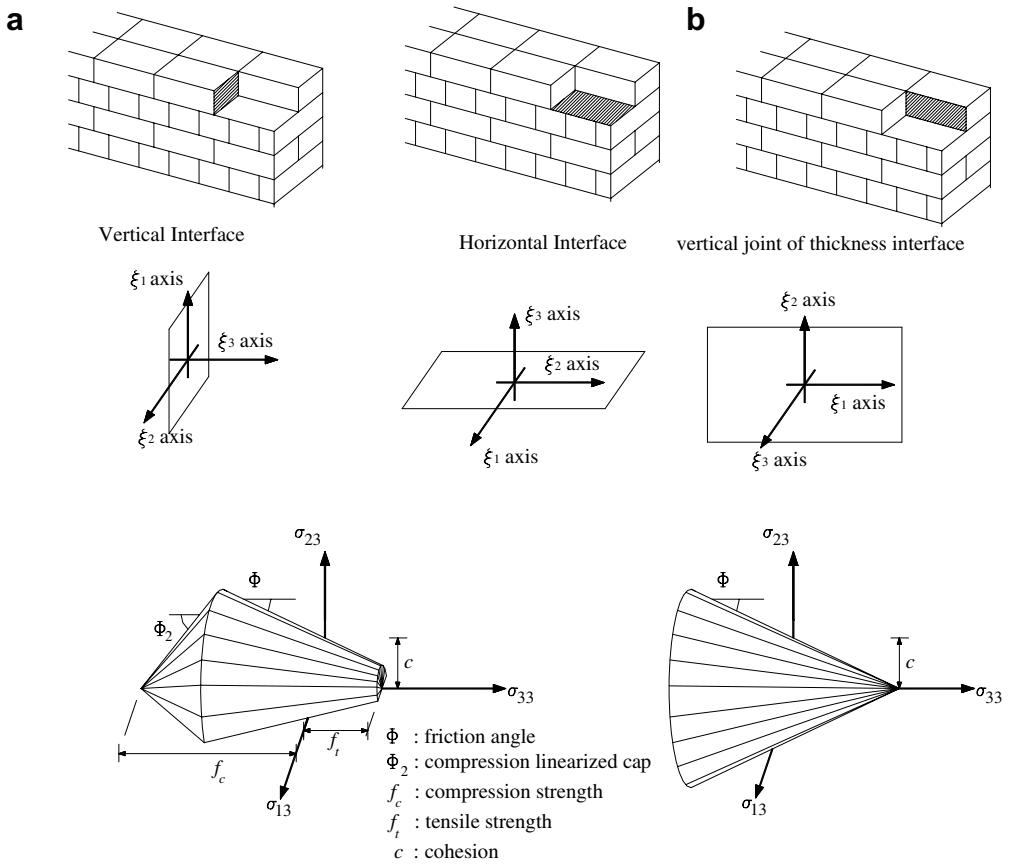

Fig. 8. Piecewise linear approximation of the failure criterion adopted for joints. (a) Mohr–Coulomb failure criterion with tension cut-off and linearized compression cap, (b) classic Mohr–Coulomb failure criterion.

Due to the linear interpolation of the displacements jump of joints reduced to interfaces (see Eq. (2)), $3 \cdot n_{\text{lin}}$ independent plastic multiplier rates are assumed as optimization variables for each interface.

As already stated in Cecchi et al. (2007), a simple set of three linear equations involving plastic multiplier rates fields $\dot{\lambda}_i^I(\xi_1, \xi_2)$ and velocity jump $[\mathbf{w}(\xi_1, \xi_2)]$ may be written in each point $\boldsymbol{\xi} = [\,\xi_1 \quad \xi_2\,] \in I$:

$$[\mathbf{w}(\xi_1, \xi_2)] = \sum_{i=1}^{n_{lin}} \dot{\lambda}_i^I(\xi_1, \xi_2) \frac{\partial \phi}{\partial \boldsymbol{\sigma}} \tag{20}$$

In Eq. (20), we assume that $[\mathbf{w}(\xi_1, \xi_2)] = [\,\Delta w_{33} \quad \Delta w_{13} \quad \Delta w_{23}\,]^{\mathrm{T}}$ is the jump of velocity field (linear in (ξ_1, ξ_2)) on the Ith interface and Δw_{ij} corresponds to the jump along the direction j, whereas $\dot{\lambda}_i^I(\xi_1, \xi_2)$ is the ith plastic multiplier rate field (linear in (ξ_1, ξ_2)) of the interface I, associated to the ith linearization plane of the failure surface.

In order to satisfy Eq. (20) for each point of the interface I, nine equality constraints for each interface have to be imposed, that corresponds to evaluate (20) in three different and not aligned positions $\boldsymbol{\xi}_k = (\xi_1^k, \xi_2^k)$ on the interface I as follows:

$$[\mathbf{w}(\xi_1^k, \xi_2^k)] = \sum_{i=1}^{n_{lin}} \dot{\lambda}_i^I(\xi_1^k, \xi_2^k) \frac{\partial \phi}{\partial \boldsymbol{\sigma}} \quad k = 1, 2, 3 \tag{21}$$

where $\dot{\lambda}_i^I(\xi_1^k, \xi_2^k)$ is the is ith plastic multiplier rate of the interface I evaluated in correspondence of $\boldsymbol{\xi}_k = (\xi_1^k, \xi_2^k)$.

Internal power dissipation occurs only on interfaces. For a generic Ith interface, such dissipation is defined as the product of the interface stress vector for the jump of velocities field, i.e. from Eq. (20):

$$\pi^I_{\text{int}} = \int_{A^I} [\mathbf{w}]^{\mathrm{T}} \boldsymbol{\sigma}\, \mathrm{d}A^I = \int_{A^I} \sum_{i=1}^{n_{lin}} \dot{\lambda}^I_i(\xi_1,\xi_2) \left[\frac{\partial \phi}{\partial \boldsymbol{\sigma}}\right]^{\mathrm{T}} \boldsymbol{\sigma}\, \mathrm{d}A^I = \frac{1}{3} \sum_{i=1}^{n_{lin}} c^I_i \sum_{k=1}^{3} \dot{\lambda}^I_i(\xi^k_1,\xi^k_2) A^I \tag{22}$$

where c^I_i is the right hand side of the ith linearization plane of the interface I failure surface.

External power dissipated can be written as $\pi_{ext} = (\Sigma_0^{\mathrm{T}} + \lambda \boldsymbol{\Sigma}_1^{\mathrm{T}})\mathbf{D}$, where Σ_0 is the vector of permanent loads, λ is the load multiplier, $\boldsymbol{\Sigma}_1^{\mathrm{T}}$ is the vector of loads dependent on the load multiplier (i.e. the optimization direction in the space of macroscopic stresses) and $\mathbf{D}$ is the vector of macroscopic kinematic descriptors. $\mathbf{D}$ collects in-plane deformation rates ($\dot{E}_{11}\,\dot{E}_{12}\,\dot{E}_{22}$), out-of-plane deformation rates ($\dot{\chi}_{11}\,\dot{\chi}_{12}\,\dot{\chi}_{22}$) and shear deformation rates ($\dot{\gamma}_{13}\,\dot{\gamma}_{23}$), see Figs. 5–7. As the amplitude of the failure mechanism is arbitrary, a further normalization condition $\boldsymbol{\Sigma}_1^{\mathrm{T}}\mathbf{D} = 1$ is usually introduced. Hence, the external power becomes linear in $\mathbf{D}$ and λ and can be written as follows $\pi_{ext} = \boldsymbol{\Sigma}_0^{\mathrm{T}}\mathbf{D} + \lambda$.

Due to the linearity of all the constraints, from Eqs. (18) and (19), a linear relation between $\mathbf{D}$ and $[\mathbf{w}(\xi_1,\xi_2)]$ may be written for each interface I as follows:

$$[\mathbf{w}(\xi_1,\xi_2)] = \mathbf{G}^I(\xi_1,\xi_2)\mathbf{D} \tag{23}$$

where $\mathbf{G}^I(\xi_1,\xi_2)$ is a 3×10 matrix which depends only on the geometry of the interface under consideration.

From Eqs. (20)–(23), the following constrained minimization problem may be finally obtained:

$$\begin{cases} \lambda = \min\limits_{\hat{\mathbf{x}}=[\mathbf{D},\lambda^I_i(\boldsymbol{\xi}_k)]} \sum\limits_{I=1}^{n^I} \pi^I_{\text{int}} - \boldsymbol{\Sigma}_0^{\mathrm{T}}\mathbf{D} \\ \boldsymbol{\Sigma}_1^{\mathrm{T}}\mathbf{D} = 1 \\ \mathbf{G}^I(\boldsymbol{\xi}_k)\mathbf{D} = [\mathbf{w}(\boldsymbol{\xi}_k)] = \sum\limits_{i=1}^{n_{lin}} \dot{\lambda}^I_i(\xi^k_1,\xi^k_2)\frac{\partial \phi}{\partial \boldsymbol{\sigma}} \quad \boldsymbol{\xi}_k \in I \end{cases} \tag{24}$$

where n^I is the total number of interfaces considered and $\hat{\mathbf{x}}$ is the vector of total optimization unknowns.

Problem (24) leads to reproduce the macroscopic combined in- and out-of-plane failure surfaces of masonry through a kinematic approach.

From a numerical point of view, macroscopic masonry failure surfaces may be obtained solving repeatedly a suitable linear programming problem derived from (24). In particular, if $\widehat{\Phi} = \widehat{\Phi}(N_{11}, N_{12}, N_{22}, M_{11}, M_{12}, M_{22}, T_{13}, T_{23})$ is the macroscopic failure surface in six dimensions for masonry and if $\Sigma = (N_{11},\ N_{12},\ N_{22},\ M_{11},\ M_{12},\ M_{22},\ T_{13},\ T_{23})$ is the vector of macroscopic unknowns ultimate strength of masonry, a 2D representation of $\widehat{\Phi}$ with respect to variables Σ_i and Σ_j can be obtained when a direction versor

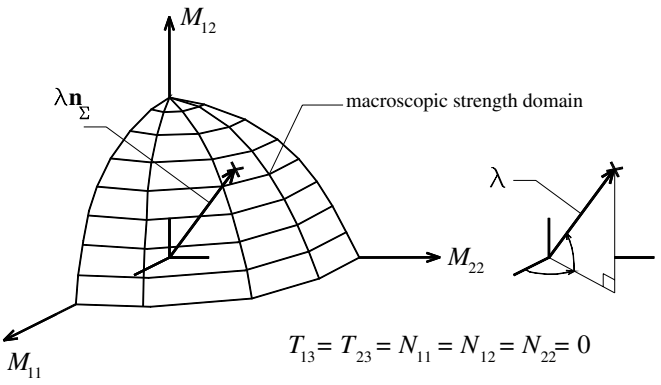

Fig. 9. Meaning of $\mathbf{n}_{\boldsymbol{\Sigma}}$ in the special 3D case $\boldsymbol{\Sigma} = (M_{11},\ M_{12},\ M_{22})$.

$\mathbf{n}_{\boldsymbol{\Sigma}}$ representing a macroscopic direction of the load such that $[\mathbf{n}_{\boldsymbol{\Sigma}}]^{\mathrm{T}}\mathbf{n}_k = 0 \ \forall \ k \neq i,j$ is chosen. Under these hypotheses, the following optimization problem is obtained from (24):

$$\begin{cases} \min\{\lambda\} = \sum_{I=1}^{n^I} \pi_{\mathrm{int}}^I - \boldsymbol{\Sigma}_0^{\mathrm{T}}\mathbf{D} \\ \mathbf{n}_{\boldsymbol{\Sigma}}^{\mathrm{T}}\mathbf{D} = 1 \quad \mathbf{n}_{\boldsymbol{\Sigma}}^{\mathrm{T}}\mathbf{n}_k = 0 \quad \forall \ k \neq i,j \\ \mathbf{G}^I(\boldsymbol{\xi}_k)\mathbf{D} = [\mathbf{w}(\boldsymbol{\xi}_k)] = \sum_{i=1}^{n_{lin}} \dot{\lambda}_i^I(\xi_1^k, \xi_2^k)\frac{\partial \phi}{\partial \boldsymbol{\sigma}} \end{cases} \tag{25}$$

where

– λ represents the collapse load when a direction $\mathbf{n}_{\boldsymbol{\Sigma}}$ in the $\boldsymbol{\Sigma}$ space (see Fig. 9) is assigned;
– $\mathbf{n}_k$ is a versor such that $\Sigma_k = \boldsymbol{\Sigma} n_k$;
– i and j represent the axes of projection of $\widehat{\Phi}$.

4. English bond out-of-plane failure surfaces

In this section, some cases of technical interest are discussed in detail, with the aim of testing both the differences in terms of strength domain when passing from a running bond to an English bond texture and the influence of shear $T_{13} - T_{23}$ macroscopic actions on the ultimate moments. Since no literature results are available for English bond behavior at collapse, only comparisons with running bond textures are discussed.

In the first example, Section 4.1, the influence of shear $T_{13} - T_{23}$ macroscopic actions on the ultimate masonry horizontal bending, torsional and vertical bending moments (i.e. M_{11}, M_{12} and M_{22}) is addressed.

Two constitutive laws are utilized and critically compared for mortar joints, consisting of a classic Mohr–Coulomb (called here Model A) and a linearized Lourenço and Rots (1997) failure criterion (denoted as Model B). Assuming $T_{13} = T_{23} = 0$, a comparison between running bond and English bond texture is also provided. Finally, two different vertical membrane loads N_{22} are applied and some sections $M_{11} - M_{22}$ and $M_{11} - M_{12}$ of the macroscopic failure surface are reported varying T_{13} and T_{23}.

In the second example, the relevant influence of vertical compressive membrane loads on M_{11}, M_{12} and M_{22} failure moments is addressed. As already pointed out for running bond textures (Cecchi et al., 2007), there is an optimal compressive load for which failure moments reach a maximum. Exceeded this optimum point, out-of-plane strength begins to decrease until membrane compressive failure occurs. Since joints failure is not possible in compression when a classic Mohr–Coulomb failure criterion is adopted, this important phenomenon can be reproduced only using Model B.

4.1. $M_{11} - M_{12} - M_{22}$ failure surface sections for different assigned $T_{13} - T_{23}$

Standard Italian UNI bricks of dimensions 5.5 cm × 12 cm × 25 cm (height × thickness × length) and mortar joints reduced to interfaces are considered. For them, both a classic Mohr–Coulomb failure criterion (Model A) and a linearized Lourenço–Rots failure criterion (Model B) are assumed and critically compared. Mechanical properties adopted for Model A and Model B are summarized in Table 1

Table 1
Mechanical properties adopted for the numerical simulations at a cell level (standard Italian UNI bricks)

Model A Mohr–Coulomb failure criterion		Model B linearized Lourenço–Rots failure criterion	
Φ	27°	c ($f_t = 1.7c$) 0.132 [N/mm^2]	f_c 3.5 [N/mm^2]
c	0.132 [N/mm^2]	Φ 27°	Φ_2 30°

The goal of the comparison is to evaluate both the influence of texture (English bond versus running bond) and the role of masonry out-of-plane shear strength $T_{13} - T_{23}$ on the macroscopic out-of-plane failure surface, in presence of different mechanical characteristics for mortar joints.

In Fig. 10a and b, respectively, several sections $M_{11} - M_{22}$ and $M_{11} - M_{12}$ of the macroscopic failure surface $\widehat{\Phi}$ are reported for Model A varying T_{13} from zero to $T_{13} = T_{13}^f$, where T_{13}^frepresents masonry failure when a pure T_{13} action is applied.

The same comparisons for Model A are illustrated in Fig. 11a and b varying T_{23} from zero to $T_{23} = T_{23}^f$.

As reported in Fig. 12, such surfaces are rather different with respect to those obtained by Cecchi et al. (2007) when a running bond texture is considered and $T_{13} = T_{23} = 0$, meaning that texture plays a not negligible role at failure, especially when out-of-plane actions are considered. In particular it must be noted that, in this case, English bond pure M_{11} ultimate bending is greater than the corresponding running bond case. This phenomenon may be justified with the shear strength of the thickness joint in conjunction with the torsional resistance of horizontal joints.

It is worth noting that authors experienced no technically meaningful differences between Model A and Model B in absence of vertical membrane compressive load, as a consequence of the fact that out-of-plane failure is mostly related to tensile cracking. Therefore only Model A results are reported for the sake of conciseness.

On the contrary, significant differences occur between the models when a vertical membrane compressive load is applied. In Fig. 13a and b, several sections $M_{11} - M_{22}$ and $M_{11} - M_{12}$ of the masonry failure strength domain are reported for Model A varying T_{13} and assuming $N_{22} = 60$ daN/mm.

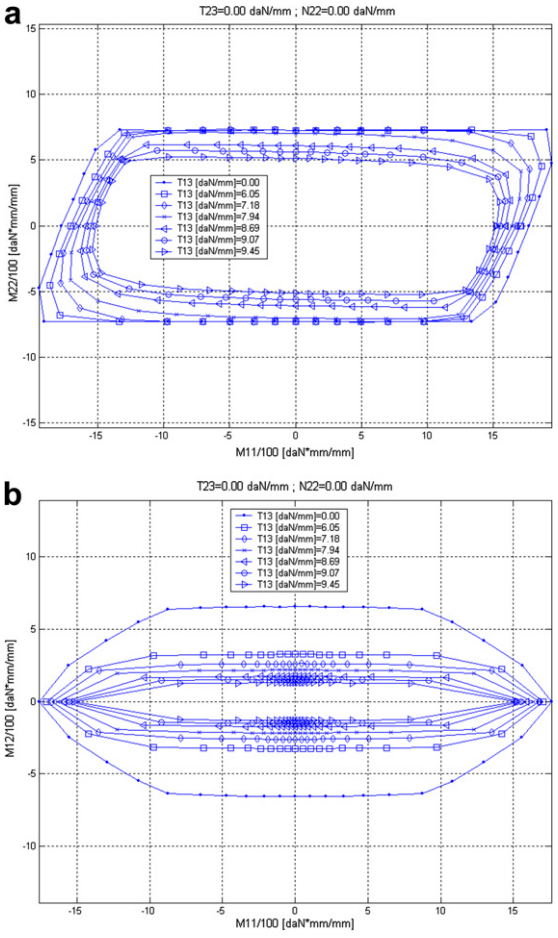

Fig. 10. Model A failure surface sections for different values of T_{13}. (a) $M_{11} - M_{22}$ sections. (b) $M_{11} - M_{12}$ sections.

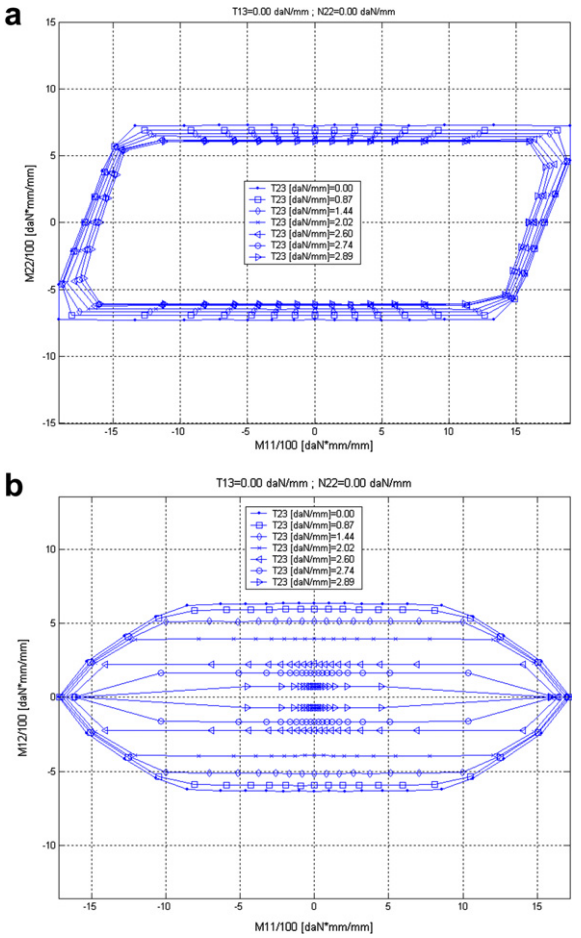

Fig. 11. Model A failure surface sections for different values of T_{23}. (a) $M_{11} - M_{22}$ sections. (b) $M_{11} - M_{12}$ sections.

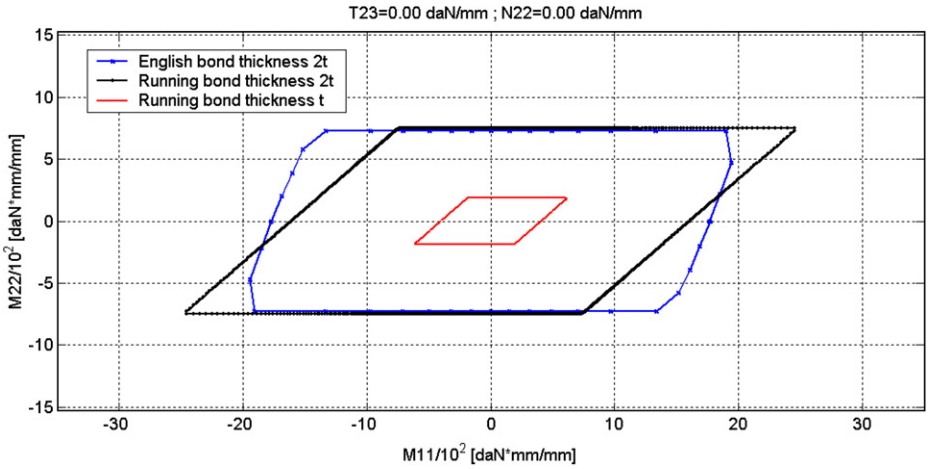

Fig. 12. Comparison among English bond texture (thickness $2t$), running bond with thickness t and running bond with thickness $2t$ $M_{11} - M_{22}$ failure surfaces ($T_{13} = T_{23} = 0$).

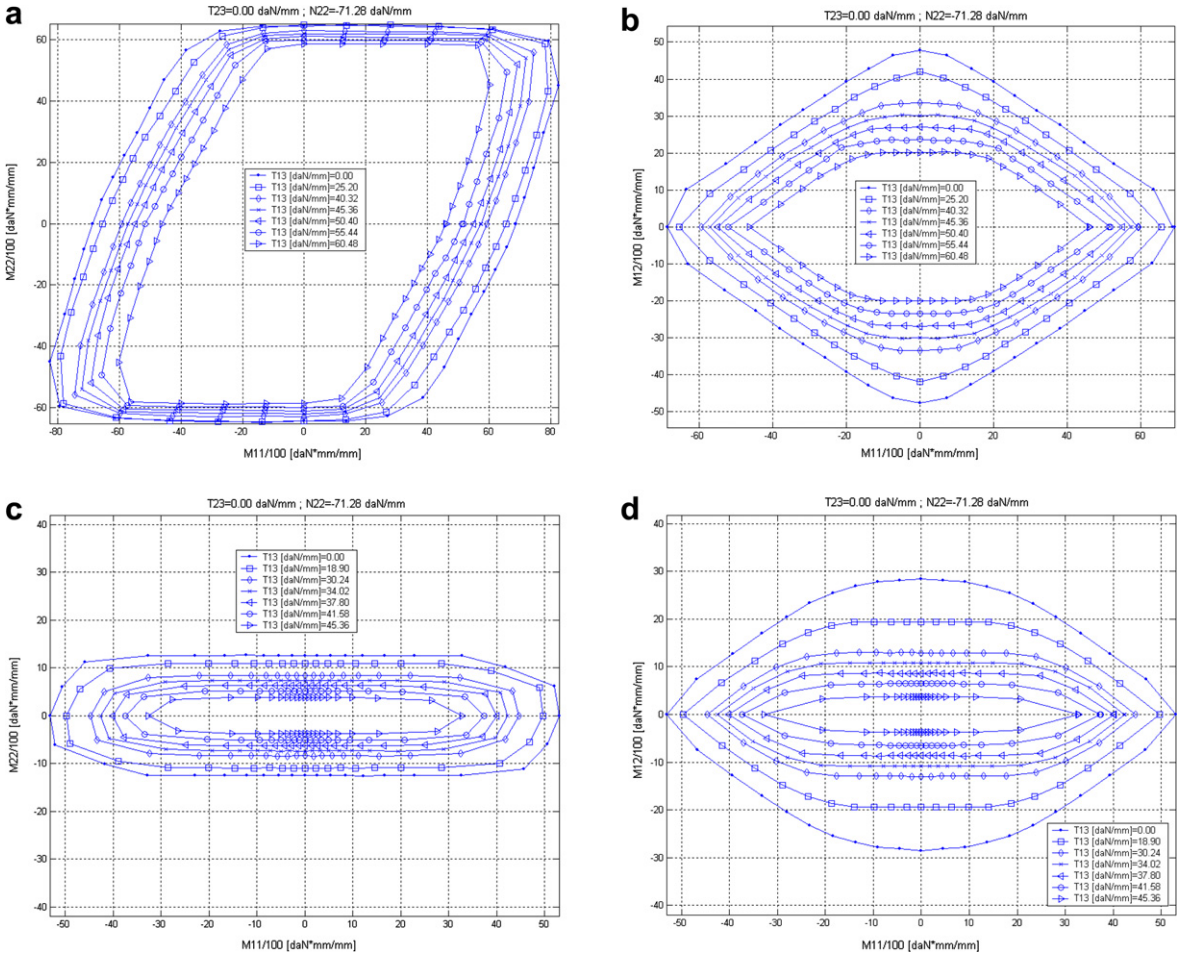

Fig. 13. (a) Model A, $M_{11} - M_{22}$ failure surfaces at different values of T_{13}. (b) Model A, $M_{11} - M_{12}$ failure surfaces at different values of T_{13}. (c) Model B, $M_{11} - M_{22}$ failure surfaces at different values of T_{13}. (d) Model B, $M_{11} - M_{12}$ failure surfaces at different values of T_{13}.

In Fig. 13c and d the same results are reported adopting Model B. As can be noted by comparing the failure curves, evident differences occur between the models. In particular the greater strength of Model A with respect to Model B under pure M_{22} ultimate bending (approximately 6000 da N/mm * mm versus 1000 da N/mm * mm) underlines that a limited compressive strength influences the ultimate out-of-plane resistance in presence of not negligible vertical membrane compressive loads.

The examples discussed underline that masonry macroscopic failure surface results dependent both on the geometrical and mechanical characteristics assumed for the components and that the proposed model is able to reproduce different macroscopic strength domains whenever different failure behaviors for the components are taken into account.

4.2. Influence of the vertical compressive membrane load

The aim of this section is to show the influence of membrane compressive loads (kept constant) on the out-of-plane masonry failure surface, when an English bond texture is considered.

For the simulations, common Italian UNI bricks of dimensions 5.5 cm × 12 cm × 25 cm (height × thickness × length) are adopted.

As in the previous case, joints are reduced to interfaces adopting for mortar both a classic Mohr–Coulomb failure surface (Model A) and a frictional-type failure surface with tensile and compressive cut-off (Model B). Mechanical characteristics adopted for both models are summarized in Table 1.

In Fig. 14a and b, respectively, several sections $M_{11} - M_{22}$ of the masonry failure surface $\widehat{\Phi}$ are reported for Model A and Model B, respectively, varying N_{22}.

In a similar way, in Fig. 14c and d the same simulations are reported representing sections $M_{11} - M_{12}$.

As it is possible to note, for both models vertical membrane load influences not only the horizontal bending moment but also the vertical one, as a consequence of the fact that also bed joints contribute to masonry vertical ultimate moment (Fig. 15).

Furthermore, the relevant influence of a vertical compressive membrane load on M_{11}, M_{12} and M_{22} failure moments is worth noting.

A comparison between Fig. 14a and b shows how a classic Mohr–Coulomb failure criterion is incapable to reproduce the actual behavior of masonry under combined compressive membrane vertical loads and out-of-plane actions, whereas the phenomenon is kept by Model B, which assumes a limited compressive strength for joints.

Obviously, this is due to the fact that a classic Mohr–Coulomb failure criterion does not provide compressive failure.

Finally, it is stressed that the choice of a failure criterion for joints with frictional behavior combined with a limited compressive and tensile strength is suitable in order to obtain technically meaningful results in agreement with experimental evidences.

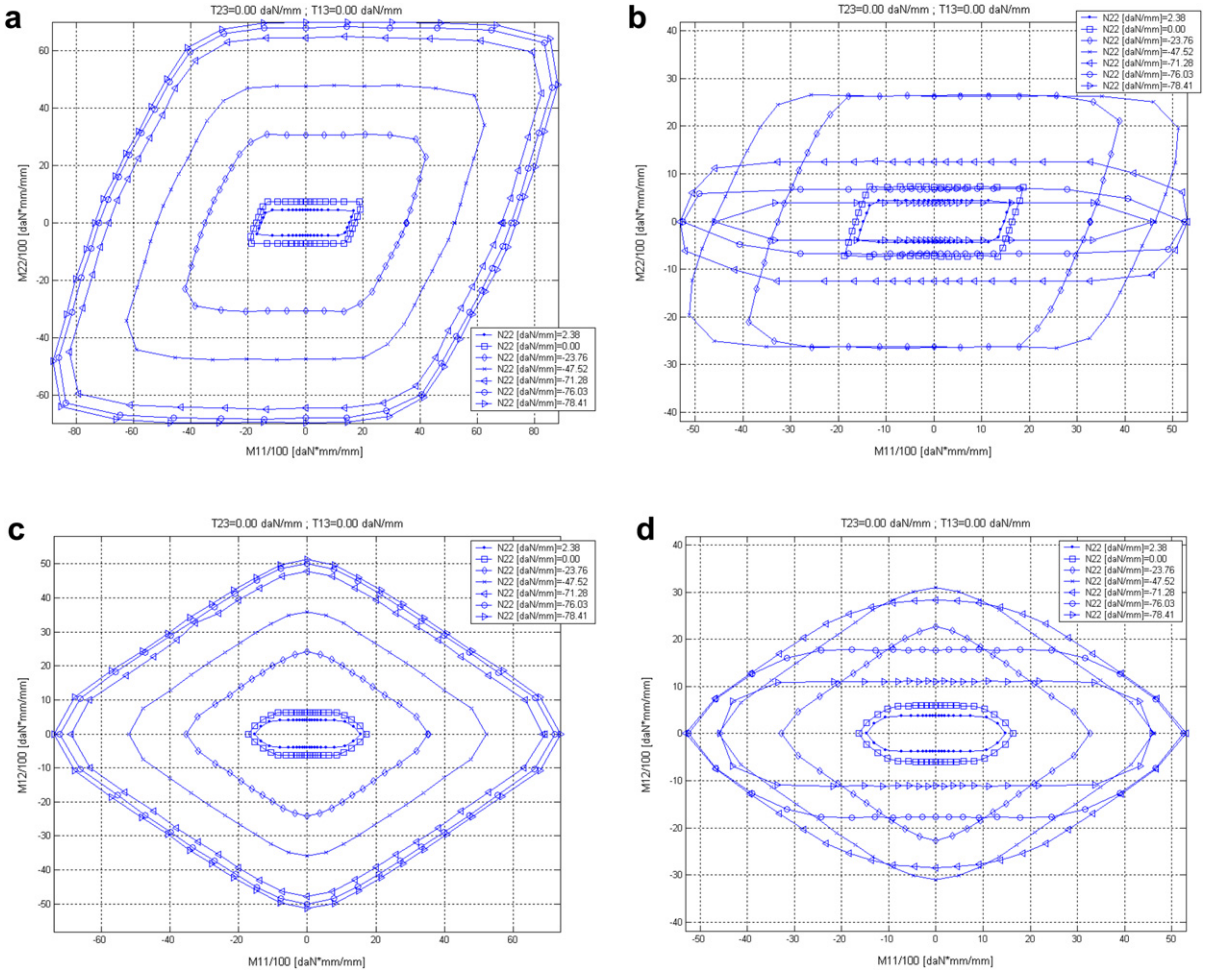

Fig. 14. (a) Model A, $M_{11} - M_{22}$ failure surfaces at different values of N_{22}. (b) Model B, $M_{11} - M_{22}$ failure surfaces at different values of N_{22}. (c) Model A, $M_{11} - M_{12}$ failure surfaces at different values of N_{22}. (d) Model B, $M_{11} - M_{12}$ failure surfaces at different values of N_{22}.

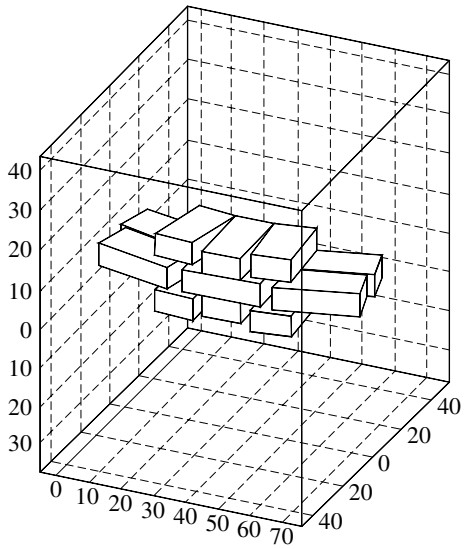

Fig. 15. Deformed shape at collapse for the elementary cell, Mohr–Coulomb failure criterion, pure M_{11} bending.

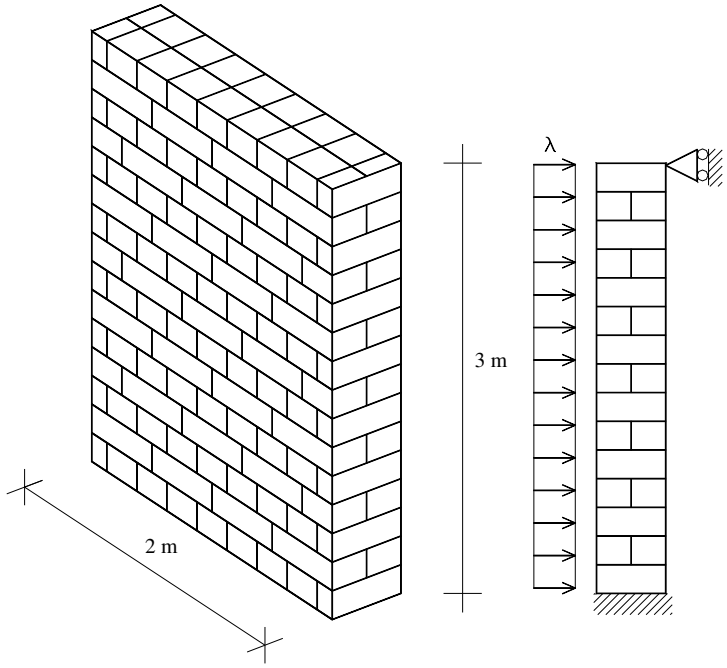

Fig. 16. English bond masonry wall in cylindrical flexion.

5. A masonry wall in cylindrical flexion

In this section, a load bearing masonry wall in cylindrical vertical flexion is analyzed with the aim of comparing failure mechanisms and limit loads provided by the Reissner–Mindlin model at hand when different bricks arrangements and different thicknesses are considered.

The masonry wall of Fig. 16 (height × width: 300 cm × 200 cm) subjected to vertical self weight and a horizontal distributed load depending on the load multiplier λ is considered. The panel is supposed clamped at the

base, whereas the restraint at the top is a simple support. No lateral restraints are applied, so that only M_{22} vertical bending moment, T_{23} shear and N_{22} membrane stress act. Two different cases are treated, the first (Case A) corresponds to a wall built with common Italian bricks of dimensions 5.5 cm × 12 cm × 25 cm (height × width × length) and arranged in English bond texture, the second (Case B) is a panel constituted by hollow/cellular concrete blocks of dimensions 20 cm × 25 cm × 50 cm (height × width × length), in which the voids percentage is neglected for simplicity. Case B is reported with the aim of underlining the importance of shear actions on thick plates. In both cases, masonry specific weight is assumed equal to 20 kN/m^3. For Case B, three walls with thickness 50 cm and different blocks disposition are investigated: the first (here denoted as Model A) is a panel arranged in English bond texture, the second (Model B) is a running bond panel, whereas the third (Model C) is composed by two running bond panels coupled in the thickness, with internal and external faces lacking in interconnecting devices along the thickness.

The aim of the structural examples presented is a comparison between the results provided by the simplified kinematic homogenization model proposed and a full 3D analysis in which bricks are assumed infinitely resistant and plastic dissipation can occur in correspondence of mortar joints reduced to interfaces.

5.1. A Reissner–Mindlin kinematic FE limit analysis approach

A 2D Reissner–Mindlin FE kinematic limit analysis model with possible plastic dissipation along the edges of adjoining elements is used at a structural level, adopting for masonry the upper bound homogenized strength domain obtained in the previous section.

In particular, we assume that a generic masonry wall is discretized by means of triangular elements. For each element E, one out-of-plane velocity unknown w_{3i}^{E} per node i is introduced, Fig. 17. In this way the velocity field is linear inside each element and plastic dissipation can occur at the interface between adjoining elements due to the combined action of bending moment, torsion and out-of-plane shear. Differently from a well known elastic FE discretization, several nodes may share the same coordinate, being each node associated with only one element. In this way, at each interface between adjacent triangles, possible jumps of velocities can occur.

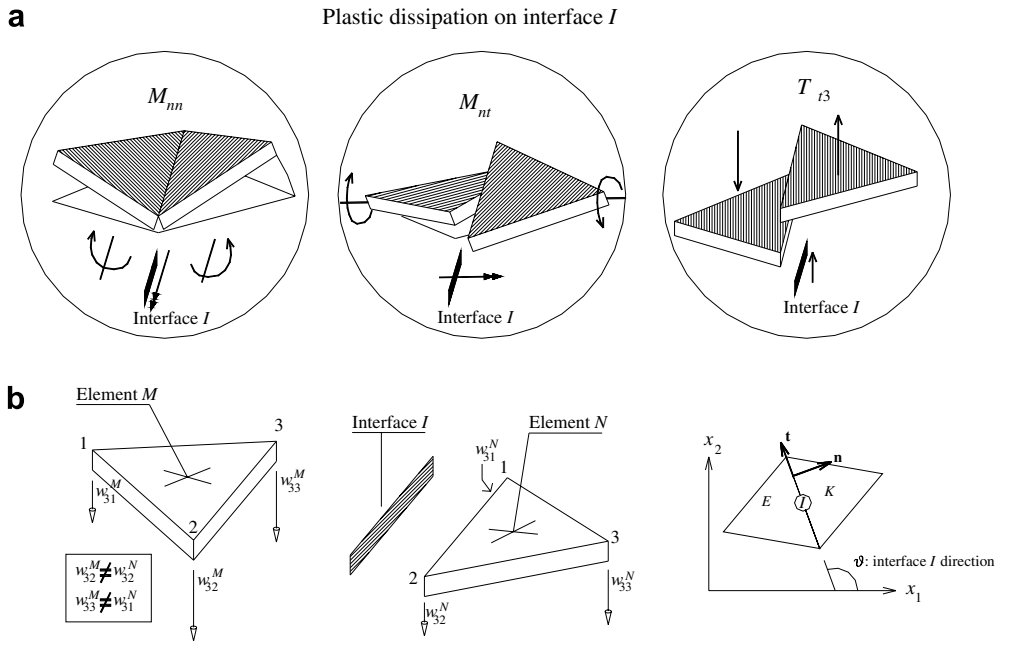

Fig. 17. Triangular element for a kinematic Reissner–Mindlin FE limit analysis. (a) Possible plastic dissipation at the interface due to bending moment, torsion and shear. (b) Field of velocities interpolation within each element and discontinuity at each interface between adjacent triangles.

Despite the fact that also in-plane velocities should be considered in the model, here only out-of-plane velocities w_{3i}^E are introduced. In this way, a drastic reduction of the total number of optimization unknowns is obtained. On the other hand, the important role of in-plane vertical compressive loads is taken into account in an approximate (but technically acceptable) way changing masonry failure surface along the height of the wall. From a practical point of view, in-plane actions are assumed as a-priori known (i.e. $N_{11} = N_{12} = 0$, $N_{22} = -\gamma(H - z) \neq 0$ where γ is the specific weight of the wall, z is the height of the interface and H is the wall height). Therefore, macroscopic masonry failure surfaces projections in the $M_{11} - M_{22} - M_{12} - T_{13} - T_{23}$ space (here denoted as $\widehat{\Phi}(M_{ij}, T_{ij}) = 0$) are used. In particular, with the aim of reducing processing time, five different linearized $\widehat{\Phi}(M_{ij}, T_{ij}) = 0$ (corresponding to different N_{22} compressive loads) are used for each of the examples treated in what follows. For each interface, the vertical coordinate (z_b) of the interface centroid is evaluated and, depending on its value, a different $\widehat{\Phi}(M_{ij}, T_{ij}) = 0$ failure surface (corresponding to $N_{22} = -\gamma(H - z_b)$) is selected. This procedure can be easily implemented in a FE limit analysis code only modifying the selection criterion of the interfaces linearized strength domain.

At each interface M and N, both constant bending rotation rates $\dot{\omega}_{N-M}^{nn}$ and a torsional rotation rates $\dot{\omega}_{N-M}^{nt}$ can occur. Furthermore, an out-of-plane jump of velocities $[w_3]$ which varies linearly along the interface is also considered. $\dot{\omega}_{N-M}^{nn}$, $\dot{\omega}_{N-M}^{nt}$ and $[w_3]$ can be easily evaluated making use of the following linear relation between nodal velocities of adjacent elements M and N (see Fig. 17):

$$\begin{aligned} &\dot{\boldsymbol{\omega}}_N = \mathbf{B}_N \mathbf{w}_3^N \\ &\dot{\omega}_{N-M}^{nt} = \frac{w_{3j}^M - w_{3i}^M}{\Gamma_I} - \frac{w_{3j}^N - w_{3k}^N}{\Gamma_I} \\ &[w_3] = (w_{3j}^M - w_{3j}^N) + \frac{x_I}{\Gamma_I}[(w_{3i}^M - w_{3k}^N) - (w_{3j}^M - w_{3j}^N)] \qquad x_I \in [\,0 \quad \Gamma_I\,] \end{aligned} \tag{26}$$

where:

- $\mathbf{w}_3^N = \left[\, w_{3i}^N \quad w_{3j}^N \quad w_{3k}^N \,\right]^{\mathrm{T}}$;
- $\mathbf{B}_N$ is a 3×3 matrix that depends only on the finite element geometry;
- $\dot{\boldsymbol{\omega}}_N = \left[\, \dot{\omega}_i^N \quad \dot{\omega}_j^N \quad \dot{\omega}_k^N \,\right]^{\mathrm{T}}$ are the side normal rotation rates, linked with $\dot{\omega}_{N-M}^{nn}$ by means of the linear equation $\dot{\omega}_{N-M}^{nn} = \dot{\omega}_i^N - \dot{\omega}_i^M$;
- Γ_I is the interface length.

Power dissipated at each interface between adjacent triangles (π^I) may be evaluated following a general approach recently presented in the technical literature for the limit analysis of plane-strain problems (see Krabbenhoft et al., 2005) and taking into account that three different elementary interface plastic dissipations can occur, related, respectively, to shear T_{nt}, bending moment M_{nn} and torsion M_{nt}.

In particular, once that function $\widehat{\Phi}(M_{ij}, T_{ij}) = 0$ is given at an interface, a rotation operator is applied to $\widehat{\Phi}$; afterwards, the simple algebraic procedure adopted in Krabbenhoft et al., 2005 is used to obtain final $T_{nt} - M_{nn} - M_{nt}$ linearized failure surfaces projections (see Krabbenhoft et al., 2005 for details).

On the other hand, external power dissipated may be written as $\pi_{ext} = (\boldsymbol{\pi}_0^{\mathrm{T}} + \lambda \boldsymbol{\pi}_1^{\mathrm{T}})\mathbf{U}$, where $\boldsymbol{\pi}_0$ is the vector of (equivalent lumped) permanent loads, λ is the load multiplier, $\boldsymbol{\pi}_1^{\mathrm{T}}$ is the vector of (lumped) variable loads and $\mathbf{U}$ is the vector of assembled nodal velocities. As the amplitude of the failure mechanism is arbitrary, a further normalization condition $\boldsymbol{\pi}_1^{\mathrm{T}}\mathbf{U} = 1$ is usually introduced. Hence, the external power becomes linear in $\mathbf{w}$ and λ, i.e. $P^{ex} = \boldsymbol{\pi}_0^{\mathrm{T}}\mathbf{w} + \lambda$.

Hence, after elementary assemblage operations and considering previously discussed constraints, the following optimization problem is obtained at a structural level:

$$\begin{cases} \min \left\{ \sum_{i=1}^{n^I} \pi^I - \boldsymbol{\pi}_0^{\mathrm{T}}\mathbf{w} \right\} \\ \text{such that} \begin{cases} \mathbf{A}^{eq}\mathbf{U} = \mathbf{A}^{eq}\left[\, \mathbf{w} \quad \tilde{\dot{\boldsymbol{\omega}}}_{nn} \quad \tilde{\dot{\boldsymbol{\omega}}}_{nt} \quad [\tilde{\mathbf{w}}_3] \quad \dot{\boldsymbol{\lambda}}^{I,ass} \,\right] = \mathbf{b}^{eq} \\ \dot{\boldsymbol{\lambda}}^{I,ass} \geqslant \mathbf{0} \end{cases} \end{cases} \tag{27}$$

where:

- $\mathbf{U} = \left[\mathbf{w} \quad \tilde{\boldsymbol{\omega}}_{nn} \quad \tilde{\boldsymbol{\omega}}_{nt} \quad [\tilde{\mathbf{w}}_3] \quad \dot{\boldsymbol{\lambda}}^{1,ass}\right]$ is the vector of global unknowns, which collects the vector of assembled nodal velocities ($\mathbf{w}$), the vector of assembled bending interface rotation rates ($\tilde{\boldsymbol{\omega}}_{nn}$), the vector of assembled torsion interface rotation rates ($\tilde{\boldsymbol{\omega}}_{nt}$), the vector of assembled jumps of velocities on interfaces ($[\tilde{\mathbf{w}}_3]$) and the vector of assembled interface plastic multiplier rates ($\dot{\boldsymbol{\lambda}}^{1,ass}$).
- $\mathbf{A}^{eq}$ is the overall constraints matrix and collects velocity and rotation boundary conditions, Eq. (26) and constraints for plastic flow in velocity discontinuities.

5.2. Heterogeneous full 3D kinematic FE limit analysis approach

Results obtained by means of the 2D Reissner–Mindlin approach proposed are compared with those obtained with a heterogeneous model. At this aim, a full 3D kinematic limit analysis program in which plastic dissipation is allowed only at the interfaces between adjoining parallelepipeds (i.e. on mortar joints reduces to interfaces), see Fig. 18, is used.

Each 3D element E (parallelepiped) is supposed infinitely resistant, thus 3 velocities unknowns $\mathbf{w}_{\mathbf{g}}^{E} = \left[w_{1-g}^{E} \quad w_{2-g}^{E} \quad w_{3-g}^{E}\right]^{\mathrm{T}}$ and 3 rotation rates $\boldsymbol{\Omega}^{E} = \left[\Omega_1^E \quad \Omega_2^E \quad \Omega_3^E\right]^{\mathrm{T}}$ per element are assumed as kinematic variables, corresponding, respectively, to $\mathbf{g}$ centroid velocity and rigid rotation rates around $\mathbf{g}$, Fig. 18.

Since velocities interpolation inside each parallelepiped is linear, jumps of velocities field on interfaces varies linearly. Hence, for each interface, nine unknowns are introduced ($\Delta\mathbf{u}^{I} = \left[\Delta u^1 \quad \Delta v_1^1 \quad \Delta v_2^1 \quad \Delta u^2 \quad \Delta v_1^2 \quad \Delta v_2^2 \Delta u^3 \Delta v_1^3 \Delta v_2^3\right]^{\mathrm{T}}$), representing the normal (Δu^i) and tangential ($\Delta v_1^i \quad \Delta v_2^i$) jumps of velocities (with respect to the interface frame of reference, suitably chosen with axes 1 and 2 on the interface plane, axis 1 parallel to the 12 edge and axis 3 perpendicular to the interface plane, Fig. 18) evaluated on nodes $i = 1$, $i = 2$ and $i = 3$ of the interface. For any pair of nodes on the interface between two adjacent parallelepipeds $M - N$, the tangential and normal velocity jumps can be written in terms of the Cartesian nodal velocities of elements $M - N$ in the following form:

$$\begin{aligned}
\Delta v_1^f &= r_{11}(w_1^{Mp} - w_1^{Ns}) + r_{12}(w_2^{Mp} - w_2^{Ns}) + r_{13}(w_3^{Mp} - w_3^{Ns}) \\
\Delta v_2^f &= r_{21}(w_1^{Mp} - w_1^{Ns}) + r_{22}(w_2^{Mp} - w_2^{Ns}) + r_{23}(w_3^{Mp} - w_3^{Ns}) \\
\Delta u^f &= r_{31}(w_1^{Mp} - w_1^{Ns}) + r_{32}(w_2^{Mp} - w_2^{Ns}) + r_{33}(w_3^{Mp} - w_3^{Ns})
\end{aligned} \tag{28}$$

where

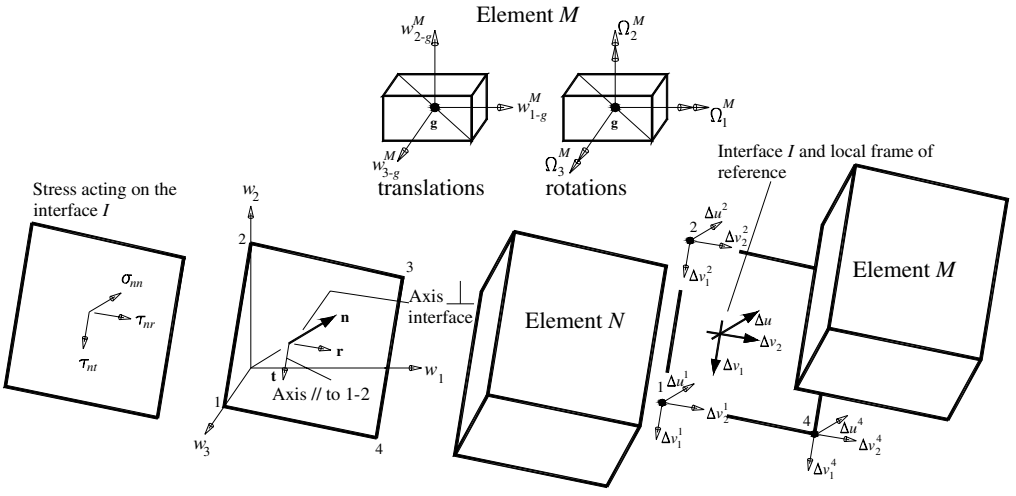

Fig. 18. 3D limit analysis model with plastic dissipation at the interfaces between adjoining elements (parallelepipeds).

– the first apex of w_i in capital letters identifies the element (M or N), while the second identifies the node number of the element ($p = k,j,q$ or $s = i,j,k$);
– $f = 1,2,3$;
– $r_{ij} = (\Delta \mathbf{v}_i/\|\Delta \mathbf{v}_i\|)^{\mathrm{T}}\mathbf{e}_j$; $(\Delta \mathbf{v}_i/\|\Delta \mathbf{v}_i\|)$ represents the versor of the ith axis of the local frame of reference, whereas $\mathbf{e}_j$ indicates the versor of the jth axis of the global frame of reference.

After elementary assemblage operations on (28), it is possible to show that, for each interface, the following equations can be written:

$$\mathbf{A}_{11}^{eq}\mathbf{w}^{Mp} + \mathbf{A}_{12}^{eq}\mathbf{w}^{Ns} + \mathbf{A}_{13}^{eq}\Delta\mathbf{u}^{I} = \mathbf{0} \tag{29}$$

where $\mathbf{w}^{Mp}$ and $\mathbf{w}^{Ns}$ are 6×1 vectors that collect centroid velocities and rotation rates of elements M and N, respectively, and $\mathbf{A}_{11}^{eq}$, $\mathbf{A}_{12}^{eq}$, $\mathbf{A}_{13}^{eq}$ are matrices which depend only on the geometry of the elements M and N.

In order to evaluate power dissipation π^I on interfaces, for each interface I a linearization of its strength domain with N_I^{pl} planes (in the form $\sigma_{nn}A_{nn-i}^I + \tau_{nt}A_{nt-i}^I + \tau_{nr}A_{nr-i}^I = B_i^I \quad i = 1,\ldots,N_I^{pl}$, see Fig. 18), obtained following what already reported in Section 3, is provided.

On the other hand, it is worth noting that recent trends in limit analysis have demonstrated that the linearization of the strength domain can be circumvented using conic programming (e.g. Makrodimopoulos and Martin, 2006; Krabbenhoft et al., 2007). This tool is more powerful with respect to LP and could lead to less expensive processing times for the 3D heterogeneous analyses, which typically required around 2 h to be processed on a PC equipped with 512 Mb ram. Nonetheless, here classic interior point LP routines are used for the sake of simplicity.

Since jump of velocities field varies linearly at each interface, it is necessary to impose plastic flow constraints on three vertices n of the rectangular interface:

$$n = 1,2,3 \begin{cases} \Delta u^n = \sum_{i=1}^{N_I^{pl}} \dot{\lambda}_i^{I,n} A_{nn-i}^I \\ \Delta v_1^n = \sum_{i=1}^{N_I^{pl}} \dot{\lambda}_i^{I,n} A_{nt-i}^I \\ \Delta v_2^n = \sum_{i=1}^{N_I^{pl}} \dot{\lambda}_i^{I,n} A_{nr-i}^I \end{cases} \tag{30}$$

where:

– Δu^n represents the jump of displacements normal to the interface;
– Δv_1^n and Δv_2^n are jumps of displacement along two perpendicular axes on the interface plane;
– $\dot{\lambda}_i^{I,n}$ is the plastic multiplier rate of the ith linearization plane of vertex n of the interface I.

Following Eq. (30), within each interface I of area A, the power dissipated is:

$$\pi^I = A/4 \sum_{n=1}^{4} \sum_{i=1}^{N_I^{pl}} \dot{\lambda}_i^{I,n} B_i^I \tag{31}$$

where node 4 results linearly dependent with respect to previous nodes.

As already discussed in this section for the 2D limit analysis approach, external power dissipation can be written in the form $\pi_{ext} = \pi_0^{\mathrm{T}}\mathbf{w} + \lambda$, once that a suitable normalization condition is introduced.

Boundary conditions on velocities are imposed in a similar way with respect to classic elastic finite elements, leading to additional equality constraints on elements velocities.

After some elementary assemblage operations, a simple linear programming problem is obtained (analogous to that reported in Milani et al., 2007), where the objective function consists in the minimization of the total internal power dissipated:

$$\begin{cases} \min \left\{ \sum_{I=1}^{N^I} \pi^I - \boldsymbol{\pi}_0^{\mathrm{T}} \mathbf{w} \right\} \\ \text{such that} \begin{cases} \mathbf{A}^{eq}\mathbf{U} = \mathbf{b}^{eq} \\ \boldsymbol{\pi}_1^{\mathrm{T}}\mathbf{U} = 1 \\ \dot{\boldsymbol{\lambda}}^{I,ass} \geqslant \mathbf{0} \end{cases} \end{cases} \tag{32}$$

where:

- N^I is the total number of interfaces in which plastic dissipation occurs;
- $\mathbf{U} = \left[\mathbf{w} \quad \Delta\mathbf{u}^{I,ass} \quad \dot{\boldsymbol{\lambda}}^{I,ass} \right]^{\mathrm{T}}$ is the vector of global unknowns, which collects the vector of assembled centroid velocities ($\mathbf{w}_{\mathbf{g}}^{E}$), the vector of assembled parallelepipeds rotations rates ($\boldsymbol{\Omega}_{\mathbf{g}}^{E}$), the vector of assembled jump of velocities on interfaces ($\Delta\mathbf{u}^{I,ass}$) and the vector of assembled interface plastic multiplier rates ($\dot{\boldsymbol{\lambda}}^{I,ass}$).
- $\mathbf{A}^{eq}$ ($\mathbf{b}^{eq}$) is the overall constraints matrix (right hands vector) and collects velocity boundary conditions, relations between velocity jumps on interfaces and elements velocities and velocity constraints for plastic flow in discontinuities.

5.3. Numerical results

For the wall under consideration, in both cases (i.e. Case A and Case B), a Lourenço–Rots failure criterion (1997) is adopted for mortar joints reduced to interfaces with friction angle $\Phi = 27°$, cohesion $c = 0.15$ N/mm^2, mortar tensile strength $f_t = 0.27$ N/mm^2, mortar compressive strength $f_c = 5$ N/mm^2 and linearized compressive cap angle $\Phi_2 = 30°$.

For what concerns the kinematic identification approach proposed, a linearization of masonry failure surface with 100 hyper-planes obtained as illustrated in the previous section is adopted. Furthermore, in the framework of the compatible identification proposed, a coarse mesh is used for the simulations, Figs. 19 and 20.

In Fig. 19, a comparison between deformed shapes at collapse obtained by means of the kinematic identification model proposed and the full 3D heterogeneous approach is presented for the wall built with common Italian bricks (Case A). As it is possible to note, perfect agreement in terms of both collapse load and failure

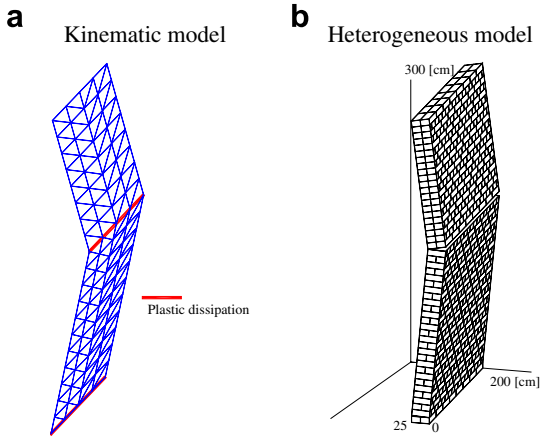

Fig. 19. Masonry panel in cylindrical flexion, English bond texture obtained with common Italian bricks of dimensions. (a) Simplified kinematic model, deformed shape at collapse. (b) Heterogeneous model, deformed shape at collapse. English bond texture, thickness 25 cm. Collapse load: 16.4 kN/m.

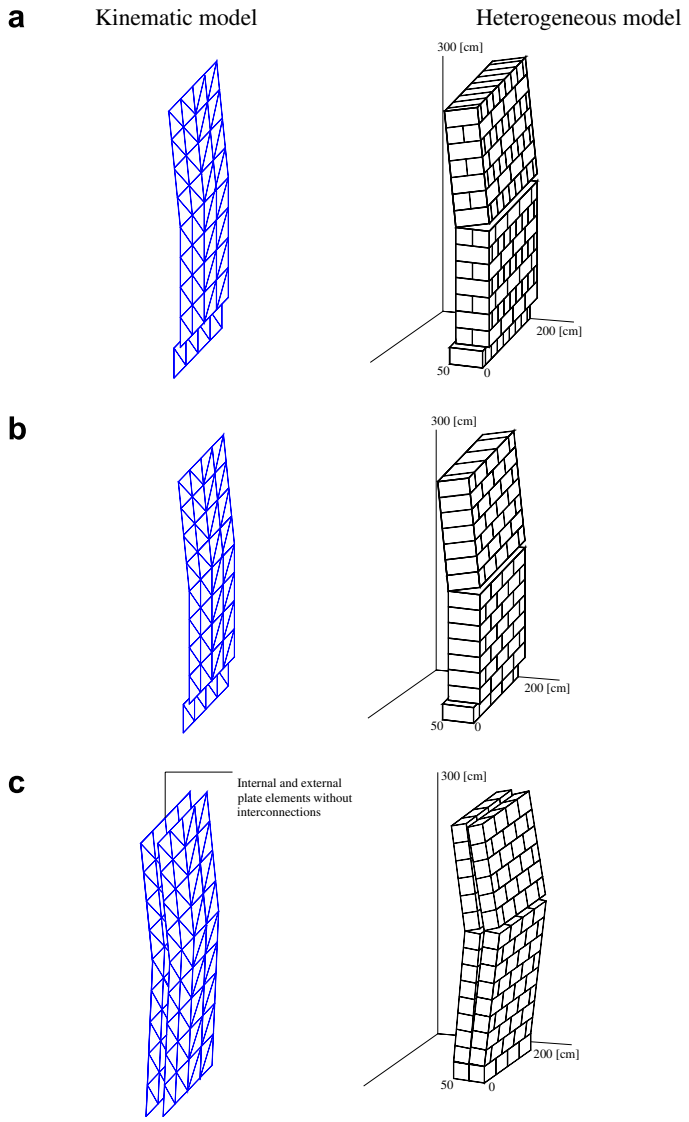

Fig. 20. Masonry panel in cylindrical flexion. Deformed shapes at collapse. (a) English bond texture, thickness 50 cm collapse linearly distributed load 58 kN/m. (b) Running bond texture, thickness 50 cm collapse linearly distributed load 58 kN/m. (c) Double running bond texture, thickness 50 cm collapse linearly distributed load 32 kN/m.

mechanism is obtained. On the other hand, it is worth noting, in the failure mechanism, the presence of two cylindrical hinges, one positioned at the base and one approximately at the centre of the wall, meaning that a Kirchhoff–Love approach is adequate in this case, due to the limited thickness of the panel.

In order to investigate the importance of shear actions on both deformed shapes at collapse and failure loads, the same results reported in Fig. 19 for Case A are reported in Fig. 20 for Case B. In particular, in Fig. 20 from a to c, failure mechanisms and failure loads obtained using both the Reissner–Mindlin model proposed and the heterogeneous approach are reported for all the bricks arrangements analyzed (i.e. Model A, Model B and Model C). As one can note, the influence of shear limited strength is particularly evident both for running bond and English bond textures, which behave exactly in the same way in cylindrical horizontal flexion.

On the other hand, a different behavior is observed for the double running bond wall, Fig. 20c, which fails for bending with separate mechanisms of the internal and external walls. In this case, for the 2D simplified

homogenized approach (Fig. 20c left), two rows of triangular elements along the thickness with possible plastic dissipation for combined bending moment, torsion and out-of-plane shear are utilized, neglecting the possible presence of shear actions at the interface between external and internal layers.

Finally, for all the arrangements analyzed (Fig. 20), the perfect agreement between heterogeneous and homogenized results is worth noting, meaning that accurate results can be obtained with the simplified kinematic model proposed.

6. A masonry slab arranged in English bond texture

In this section, the capabilities of the compatible model proposed in the present paper are tested at a structural level on a real 2D example. In particular, an English bond masonry slab out-of-plane loaded and constrained at three edges (simple supports on vertical edges and fixed base, Fig. 21) is analyzed by means of a number of different FE limit analysis models.

The first model (here denoted as Model A) relies in the 3D heterogeneous approach with infinitely resistant bricks, whereas the second (Model B) is a FE kinematic limit analysis approach based on Reissner–Mindlin plate hypotheses. Both a kinematic homogeneous (Model B_Hom) and a heterogeneous approach (Model B_Het) are proposed. Both Model A and Model B have already been presented in the previous sections. A final Model C is used to validate the results obtained, consisting in a Kirchhoff–Love homogenized approach (see Milani et al., 2006b for further details), suitable only for thin plates.

In order to test the capabilities of the approaches presented, a masonry wall of dimensions 400 cm × 320 cm × 50 cm (height × width × length) arranged in English bond texture, simply supported at two edges with the base clamped, Fig. 21, is considered. The wall is assumed built in English bond texture with cellular concrete blocks of dimensions 50 cm × 20 cm × 25 cm (height × width × length) and specific weight equal to 20 kN/m^3. Here the percentage of voids is neglected for the sake of simplicity. Despite the fact that, as a rule, load bearing walls thickness t varies from 20 to 40 cm, we assume here t equal to 50 cm with the sole aim of underlining that a Reissner–Mindlin approach should be used instead of a Kirchhoff–Love one when thick slabs are considered. The wall is supposed loaded with a distributed out-of-plane pressure until failure. For joints a Lourenço–Rots failure criterion is adopted, with mechanical properties summarized in Table 2. Such values represent typical strength values available in the technical literature.

Table 3 shows a comparison among the collapse loads obtained with Model A, Model B_Hom and Model C_Het, whereas in Fig. 22a comparison between deformed shapes at collapse obtained with all the models is

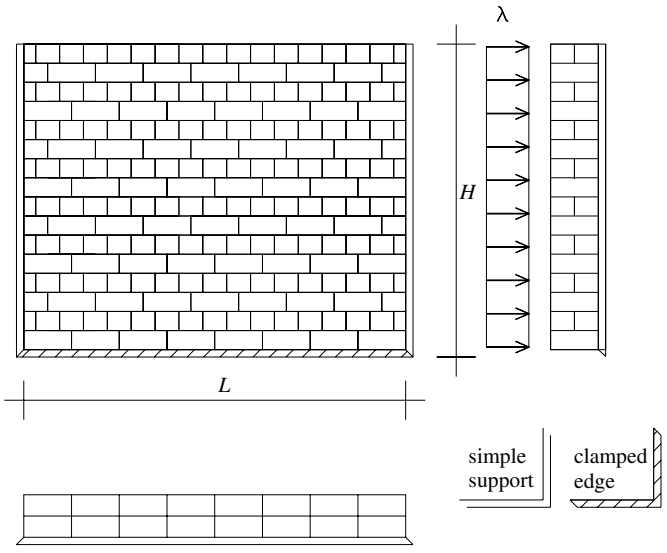

Fig. 21. Rectangular panel clamped at the base and simply supported at two edges. Geometry.

Table 2
Masonry slab constrained at three edges

f_t [N/mm^2]	c	Φ	f_c [N/mm^2]	Φ_2
0.15	0.8 f_t	30°	5	30°

Mechanical characteristics assumed for mortar joints f_t, mortar tension cut-off; c, mortar cohesion; Φ, mortar friction angle; f_c, mortar compressive strength; Φ_2, shape of the linearized compressive cap.

Table 3
Masonry slab constrained at three edges

English bond texture $t = 50$ cm, ultimate pressure [kN/m^2]	
22.12	Full 3D heterogeneous model (Model A)
23.40	Reissner–Mindlin homogeneous kinematic model (Model B_Hom)
26.10	Reissner–Mindlin heterogeneous model (Model B_Het)

English bond bricks disposition. Comparison among failure loads obtained using a full heterogeneous 3D model, a 2D kinematic homogeneous Reissner–Mindlin FE limit analysis approach and a 2D heterogeneous Reissner–Mindlin FE limit analysis model.

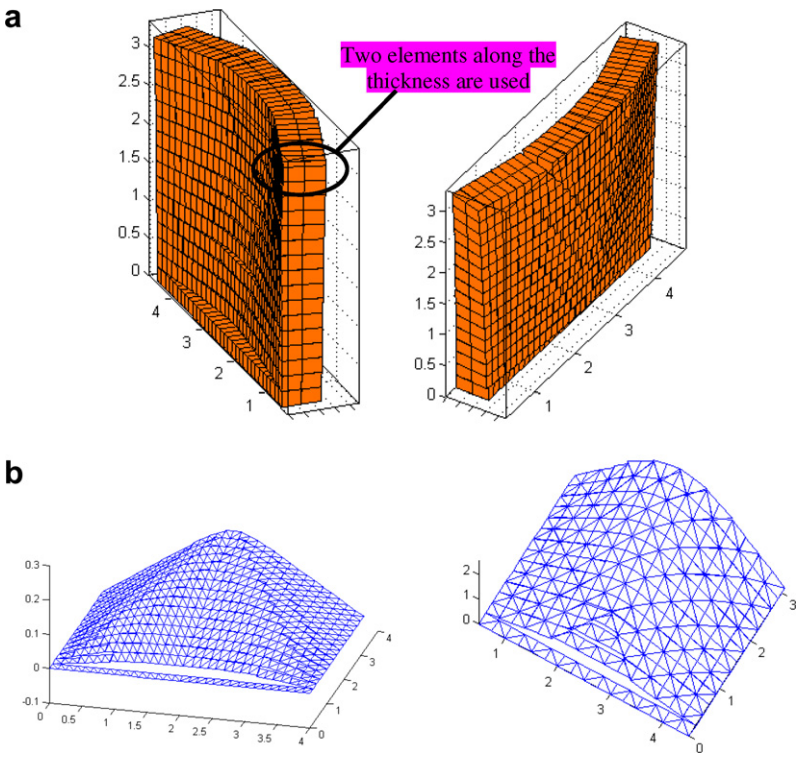

Fig. 22. Masonry panel simply supported at three edges. Deformed shapes at collapse (Model A). (a) English bond texture, 3D heterogeneous approach. (b) English bond texture, heterogeneous 2D (left) and simplified homogeneous kinematic approach (right).

reported. Here, it is worth mentioning that for Model B_Het we assume, see Milani et al. (2007), 2D Reissner–Mindlin plate hypotheses with plastic dissipation only on joints reduced to interfaces. Furthermore, vertical joints disposed along the thickness are not taken into account. Therefore, a collapse load greater than those obtained with Model A and Model B_Hom is expected, as confirmed by Table 3.

As it is possible to note from a comparison between Table 3 and Fig. 22, the compatible identification approach (Model B_Hom) gives results in excellent agreement with the full 3D heterogeneous one (Model A). On the other hand, for both models it is particularly evident the influence of the limited shear strength,

especially at the base of the wall where out-of-plane tangential actions reach their maximum value. The limited out-of-plane strength is well reproduced also by Model B_Het, which furnishes a collapse load slightly greater.

For what concerns mesh dependence of the models used, it is worth noting that mesh orientation and size of triangular elements used in Model B_Hom (Fig. 22b) can play a relatively important role when out-of-plane models with plastic dissipation only at the interfaces between adjoining elements are adopted. On the other hand, it has been shown with a number of examples (see Milani et al., 2006b; Lourenço et al., in press) that quite refined meshes with undistorted elements (i.e. ≈1/10 of the edge length, as is the case here treated) give technically acceptable results, with differences on collapse loads obtained with classic elasto-plastic approaches less than 10%.

In order to evaluate the importance of both bricks texture and panel thickness, a further comparison is here discussed, consisting in the same panel with the same loads and boundary conditions but with thickness 25 cm and 50 cm, respectively, and arranged in running bond texture. Fig. 23 shows deformed shapes at collapse for the wall under consideration (thickness 25 cm) obtained with a 3D heterogeneous mesh (Model A), the heterogeneous Reissner–Mindlin approach (Model B_Het) and the homogeneous kinematic Reissner–Mindlin model (Model B_Hom). As one can note from Fig. 23c, where Model B_Hom deformed shape at collapse is shown, a Kirchhoff–Love behavior is obtained when thin plates are considered (i.e. Model B_Hom coincides with Model C). In Table 4, a synopsis of the failure loads obtained using all the models discussed (i.e. full 3D heterogeneous limit analysis, 2D heterogeneous and homogeneous kinematic Reissner–Mindlin approaches, 2D homogenized Kirchhoff–Love models) is reported. A critical comparison among Table 3, Table 4 Fig. 23 and Fig. 23 permits to underlined the following key aspects of the problem:

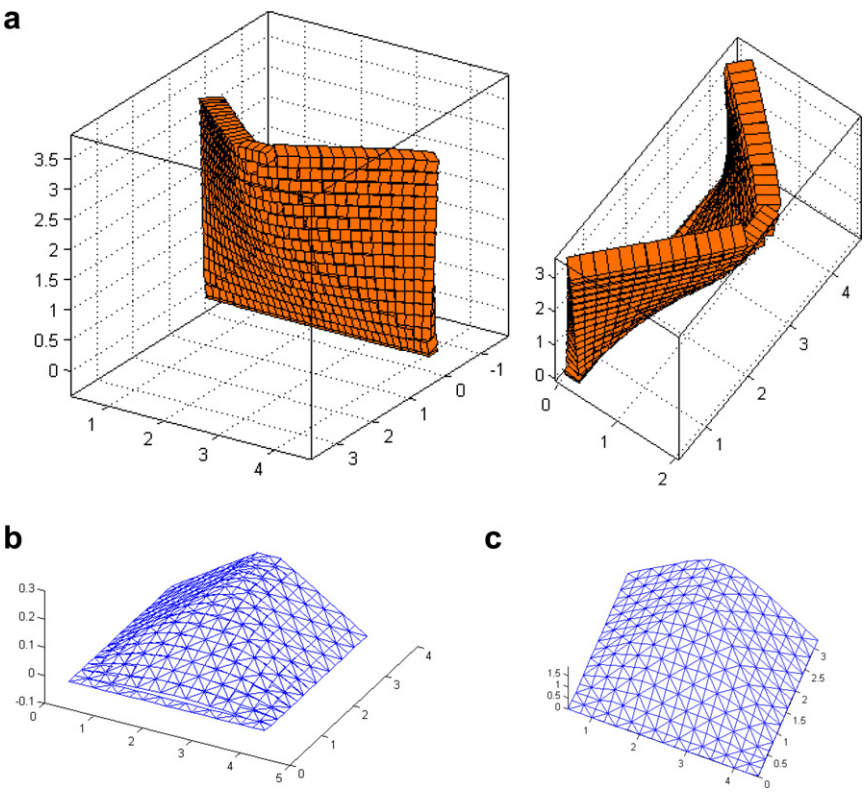

Fig. 23. Masonry slab simply supported at three edges, running bond texture with thickness 25 cm. Deformed shapes at collapse and failure pressure. (a) Full 3D heterogeneous approach (Model A). (b) Reissner–Mindlin 2D heterogeneous approach (Model B_Het). (c) Kinematic homogeneous 2D Reissner–Mindlin approach (Model B_Hom).

Table 4
Masonry slab constrained at three edges

Running bond texture, ultimate pressure [kN/m^2]		
Thickness $t = 25$ cm	Model adopted	Thickness $t = 50$ cm
8.01	Heterogeneous 3D model (Model A)	29.91
8.15	Heterogeneous Reissner–Mindlin model (Model B_Het)	30.19
8.12	Kinematic homogeneous Reissner–Mindlin model (Model B_Hom)	29.91
9.69	Homogenized 2D Kirchhoff–Love model (Model C)	38.75

Running bond bricks disposition. Comparison between failure loads obtained using a full heterogeneous 3D model and a number of 2D Reissner–Mindlin and Kirchhoff–Love FE limit analysis models.

1. Reissner–Mindlin FE limit analysis models give reliable results if compared with full expensive 3D heterogeneous approaches when thick plates are considered. This is particularly evident from the deformed shape at collapse, which exhibits out-of-plane sliding of the bricks;
2. The compatible identification proposed in this paper can be applied for multi-wythes masonry panels arranged in English bond texture. When complex 2D structural problems are treated, kinematic macroscopic failure surfaces can be implemented in standard 2D limit analysis codes. Such approach is able to give satisfactory results if compared with expensive heterogeneous approaches.

References

Begg, D., Fishwick, R., 1995. Numerical analysis of rigid block structures including sliding. In: J. Middleton, G. Pande (Eds.), Computer Methods in Structural Masonry, vol. 3, pp. 177–183.

Calvi, G.M., Magenes, G., Pavese, A., 1992. Experimental and numerical investigation on a brick masonry building prototype – Report 1.1 – Design of the experimental tests. D.M.S report, Università di Pavia.

Cecchi, A., Milani, G., Tralli, A., 2007. A Reissner–Mindlin limit analysis model for out-of-plane loaded running bond masonry walls. International Journal of Solids and Structures 44 (5), 1438–1460.

Cecchi, A., Rizzi, N.L., 2003. Analisi in più parametri perturbativi per murature a struttura regolare: identificazione 3D con modelli 2D di piastra. In: Proc. XVI congresso AIMETA di meccanica teorica e applicata, Ferrara (Italy) 9–12 September.

Cecchi, A., Sab, K., 2004. A comparison between a 3D discrete model and two homogenised plate models for periodic elastic brickwork. International Journal of Solids and Structures 41 (9-10), 2259–2276.

de Buhan, P., de Felice, G., 1997. A homogenisation approach to the ultimate strength of brick masonry. Journal of the Mechanics and Physics of Solids 45 (7), 1085–1104.

Drescher, A., Detournay, E., 1993. Limit load in translation failure mechanisms for associative and non-associative materials. Geotechnique 43 (3), 443–456.

Ferris, M., Tin-Loi, F., 2001. Limit analysis of frictional block assemblies as a mathematical program with complementarity constraints. International Journal of Mechanical Sciences 43, 209–224.

Krabbenhoft, K., Lyamin, A.V., Hjiaj, M., Sloan, S.W., 2005. A new discontinuous upper bound limit analysis formulation. International Journal for Numerical Methods in Engineering 63, 1069–1088.

Krabbenhoft, K., Lyamin, A.V., Sloan, S.W., 2007. Formulation and solution of some plasticity problems as conic programs. International Journal of Solids and Structures 44, 1533–1549.

Lourenço, P.B., Rots, J., 1997. A multi-surface interface model for the analysis of masonry structures. Journal of Engineering Mechanics ASCE 123 (7), 660–668.

Lourenço, P.B., Milani, G., Tralli, A., Zucchini, A., 2007. Analysis of masonry structures: review and new trends of homogenisation techniques. Canadian Journal of Civil Engineering, in press.

Makrodimopoulos, A., Martin, C.M., 2006. Lower bound limit analysis of cohesive-frictional materials using second-order cone programming. International Journal for Numerical Methods in Engineering 66 (4), 604–634.

Milani, G., Lourenço, P.B., Tralli, A., 2006a. Homogenised limit analysis of masonry walls. Part I: failure surfaces. Computers and Structures 84 (3-4), 181–195.

Milani, G., Lourenço, P.B., Tralli, A., 2006b. Homogenization approach for the limit analysis of out-of-plane loaded masonry walls. ASCE Journal of Structural Engineering 132 (10), 1650–1663.

Milani, G., Zuccarello, A., Olivito, R.S., Tralli, A., 2007. Heterogeneous upper-bound finite element limit analysis of masonry walls out-of-plane loaded. Computational Mechanics 40, 911–931.

O.P.C.M. 3431/05 09/05/2005, 2005. Ulteriori modifiche ed integrazioni all'OPCM 3274/03 (in Italian) & O.P.C.M. 3274, 20/03/2003, Primi elementi in materia di criteri generali per la classificazione sismica del territorio nazionale e di normative tecniche per le costruzioni in zona sismica (in Italian).

Orduña, A., Lourenço, P.B., 2005. Three-dimensional limit analysis of rigid blocks assemblages. Part I: torsion failure on frictional joints and limit analysis formulation. International Journal for Solids and Structures 42 (18–19), 5140–5160.

Page, A.W., 1981. A biaxial failure criterion for brick masonry in the tension–tension range. International Journal of Masonry 1, 26–30.

Sab, K., 2003. design of thin periodic plates by a homogenisation technique and an application to masonry walls. CR Mechanique 331, 641–646.

Spence, R., Coburn, A., 1992. Strengthening building of stone masonry to resist earthquakes. Meccanica 27, 213–221.

Suquet, P., 1983. Analyse limite et homogeneisation. Comptes Rendus de l'Academie des Sciences – Series IIB – Mechanics 296, 1355–1358.

Sutcliffe, D.J., Yu, H.S., Page, A.W., 2001. Lower bound limit analysis of unreinforced masonry shear walls. Computers and Structures 79, 1295–1312.